Previous GMSA showed that MafG homodimer strongly binds to MARE25, but scarcely to MARE23, suggesting that the flanking sequence of MARE is critical for DNA binding of Maf family proteins (Kataoka *et al.* 1995).

A single-stranded DNA array with the two sequences, MARE25 and MARE23, was fabricated and sequentially exposed to 1 μM of their complementary oligonucleotides and 125 nM of MafG homodimer. Figure 3A,B show binding profiles simultaneously observed at three test spots, MARE25, MARE23 and blank (a spot with free maleimido groups), as well as one background area (a spot with free PEG-thiol groups) by SPR imaging technique. The increases of SPR signals by the addition of the complementary oligonucleotides were detected in both spots of MARE25 and MARE23, which suggests the generation of double stranded DNAs by hybridization. Importantly, no cross-hybridization was observed in these processes, indicating that the arrays were fabricated properly without base mis-pairing. When MafG was applied to the flow on the SSMCC-immobilized array, the SPR signals were increased marginally at both MARE25 and MARE23 spots, which indicates that MafG did not interact efficiently with both DNAs under this condition (Fig. 3A). On the contrary, a robust increase of SPR signal was observed for MARE25, but not for MARE23, on the NHS-PEG-MAL-immobilized array (Fig. 3B). The results were in very good agreement with the previous GMSA results, demonstrating that specific DNA-binding of MafG homodimer was reproduced on the NHS-PEG-MAL-immobilized array, but not on the SSMCC-immobilized array. Therefore, the NHS-PEG-MAL was chosen in this study for the analysis of interaction between MafG and MARE-related sequences.

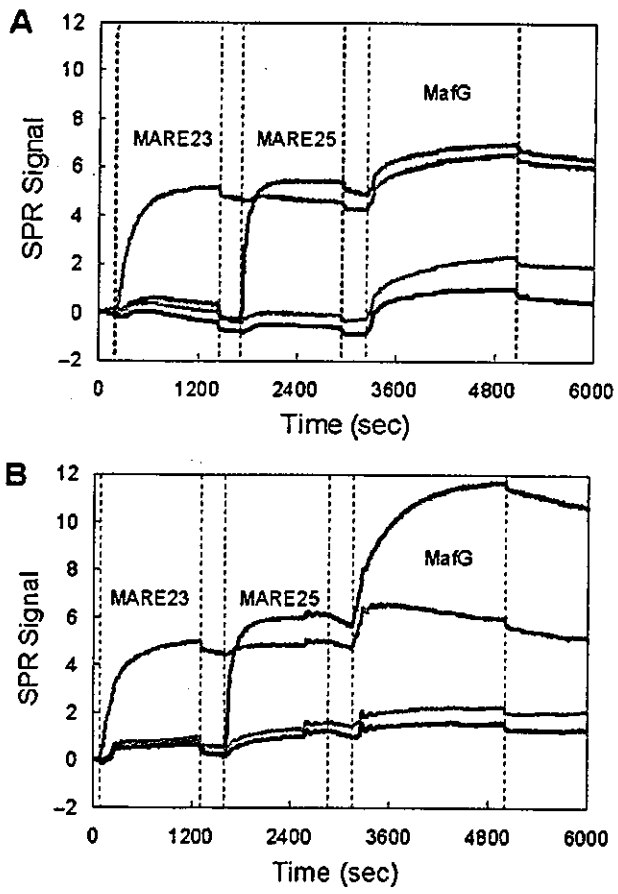


**Figure 3** Sequential DNA immobilization method for generation of double-stranded DNAs on chip surface. The SPR signal changes by the exposure to 1 μM of complementary oligonucleotides of MARE25 and MARE23, and subsequently to 125 nM of MafG homodimer. The changes are monitored at MARE25 (blue), MARE23 (purple), blank (green), and background (black). Single-strand DNA was immobilized on the surface via (A) SSMCC and (B) NHS-PEG-MAL.

### Salt concentration affects kinetic SPR measurements

Among various components of the SPR binding buffer, we found that the salt concentration had the greatest influence on the occurrence of nonspecific binding of transcription factors. We measured the SPR signals after continuous MafG application for 30 min at different sodium chloride concentrations from 150 mM to 300 mM (Table 2). When the sodium chloride concentration is 150 mM or less, the nonspecific binding was observed at the blank spot and PEG background on the chip, judged from the smaller value of $S_1/N$ ratio (Table 2 and data not shown). In contrast, when 300 mM sodium chloride was applied, $S_1$ value (Table 2) became low, suggesting that the specific binding was inhibited. We therefore utilized intermediate concentration of sodium chloride, i.e. 200 mM, for the MafG analysis.

Under the final binding condition (20 mM HEPES-HCl (pH 7.9), 200 mM NaCl, 4 mM $MgCl_2$, 1 mM EDTA, and 100 μg/ml BSA), MafG sufficiently bound to MARE25, but not MARE23, and the kinetic data were obtained for MARE25 as $k_a$ (association rate constant) = $4.11 \times 10^4$ ($M^{-1} s^{-1}$), $k_d$ (dissociation rate constant) = $1.49 \times 10^{-4}$ ($s^{-1}$), and $K_D$ (dissociation constant) = $3.63 \times 10^{-9}$ (M) by curve fitting calculation from simple binding model (George *et al.* 1995).

### Interaction between MafG and MARE-related sequences examined on one chip

We then evaluated a double-stranded DNA array fabricated by the new immobilization method. Each pair of complementary oligonucleotides was first annealed

**Table 2** Influence of salt concentration on SPR signals

| NaCl concentration | SPR signal | | | | |
|---|---|---|---|---|---|
| | MARE25 ($S_1$†) | MARE23 ($S_2$†) | Background (N†) | $S_1/S_2$ | $S_1/N$ |
| 150 mM | 13.40 ± 1.70 | 6.60 ± 0.85 | 5.44 ± 0.56 | 2.04 | 2.47 |
| 200 mM | 20.00 ± 3.90 | 4.57 ± 1.83 | 1.24 ± 0.02 | 4.38 | 16.10 |
| 300 mM | 8.07 ± 2.49 | 1.24 ± 0.21 | 1.80 ± 1.78 | 6.51 | 4.50 |

†SPR signals obtained after continuous MafG application for 30 min. $S_1$, $S_2$ and N are the values at the spots of MARE25, MARE23 and the background area, respectively.

and then immobilized on the surface of a gold chip. The double-stranded oligonucleotides were spotted by an automated spotter and immobilized through the thiol-modified 5′-protruding end on the gold surface via NHS-PEG-MAL. We chose four MARE-related sequences found in the regulatory regions of four endogenous genes (Table 1), including human NQO1 (hNQO1m MARE; Venugopal & Jaiswal 1996), mouse GSTy (mGSTY MARE; Itoh *et al.* 1997), human β-globin gene (hBglHS4 MARE; Stamatoyannopoulos *et al.* 1995), and human rhodopsin gene (hOPSIN MARE; Kumar *et al.* 1996). The importance of these MAREs has been examined functionally in co-transfection-transactivation analyses. The human NQO1 MARE has an altered flanking region on one side, which is similar to human β-globin MARE. To examine MAREs encompassing various categories, we modified flanking sequence of human NQO1 MARE so that the crucial 'G' in the flanking region is conserved symmetrically (Table 1). For this reason, we named the DNA as hNQO1m. In addition to these MAREs, both MARE25 and MARE23 were spotted as a positive and negative control, respectively.

The chip with the immobilized double-stranded DNAs was placed to the SPR imaging instrument, and 125 nM of MafG homodimer was applied for the DNA-protein association analysis. The SPR signal profiles of association and dissociation were observed for 1800 s with MafG-containing buffer and for the following 1200 s with the blank buffer, respectively. These results are shown in the conventional binding curves in Fig. 4A. To visualize the results more effectively, we also calculated the signals utilizing Scion Image software and the results are shown in the form of SPR difference image in Fig. 4B. The association and dissociation rate constants were calculated from the curve profiles (Fig. 4, $n = 3$) and summarized in Table 3. Although $k_a$ and $k_d$ values obtained from the single-stranded DNA array were slightly lower than those obtained from the double-stranded array, $K_D$ values of MARE25 were almost the same in the two distinct

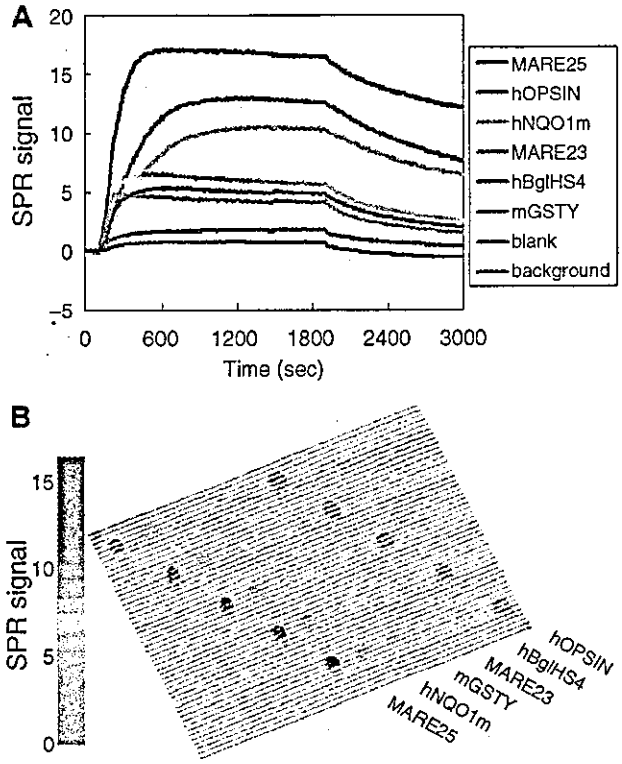


**Figure 4** Interaction between MafG and MARE-related sequences examined on one chip with a double-stranded DNA array. (A) The SPR signal changes by the exposure to 125 nM MafG homodimer on the double-stranded DNA array where six MARE-like sequences are immobilized. The buffer with MafG started to flow at 0 s and was terminated at time 1800 s. The buffer without MafG was replaced and continued for the following 1200 s. Representative binding curves, each of which was obtained from a single spot, are shown. Three independent experiments were performed, and the kinetic data were calculated (see Table 3). (B) SPR difference image showing the binding of the MafG homodimer on to the double-stranded DNA array after the exposure to 125 nM MafG. Five independent spots of each oligonucleotide were generated for visualizing a representative image.

**Table 3** Kinetic values of interactions between MafG homodimer and MARE-related sequences calculated from SPR profiles and GMSA

| | SPR average | | | GMSA |
|---|---|---|---|---|
| | $k_a$ [$M^{-1}$ $s^{-1}$] $10^5$ | $k_d$ [$s^{-1}$] $10^{-4}$ | $K_D$ [M] $10^{-9}$ | $K_D$ [M] $10^{-7}$ |
| MARE25 | 1.36 ± 0.32 | 3.13 ± 0.66 | 2.50 ± 1.02 | 2.49 ± 0.06 |
| hOPSIN | 0.50 ± 0.06 | 3.72 ± 0.30 | 7.68 ± 1.17 | 2.52 ± 0.05 |
| hNQO1m | 0.39 ± 0.04 | 3.24 ± 0.36 | 8.59 ± 1.75 | 2.73 ± 0.13 |
| mGSTY | ND | ND | ND | ND |
| MARE23 | ND | ND | ND | ND |
| hBglHS4 | ND | ND | ND | ND |

SPR was measured 3 times, and the average and standard deviation are shown. ND not able to determine. $k_a$, association rate constant; $k_d$, dissociation rate constant; $K_D$, dissociation constant.

arrays (see above and Fig. 3B). A reason for the difference in $k_a$ and $k_d$ values is unknown, but the similar $K_D$ values suggest that the double-stranded DNA was properly immobilized on the surface without being denatured. The SPR difference image (Fig. 4B) was calculated from the SPR signals before and after exposure to MafG, and these signals represent that MafG properly binds to the spots. We interpret that MafG binds to MAREs specifically, since the signals on PEG background and a blank spot, where NHS-PEG-MAL is immobilized, are negligible. These results thus demonstrate successful establishment of a modified surface immobilization procedure for a double-stranded DNA array fabrication.

Kinetic data were calculated for the sequences to which substantial MafG binding was observed. Since MafG binds to DNA exclusively through forming a homodimer, it seems quite likely that observed kinetic data represent the interaction between MafG homodimer and double-stranded oligonucleotide containing MARE-related sequences. Of the six MARE and related sequences, sufficient amount of MafG interacted with MARE25, hOPSIN MARE, and hNQO1m MARE (Fig. 4). MARE25 displayed the highest affinity, and hOPSIN and hNQO1m MAREs are the next (Table 3). hOPSIN MARE has two base replacements in the MARE consensus sequence of MARE25; one is in the centre of the core region and the other is in the end of the flanking region. On the contrary, hNQO1m MARE possesses well conserved core region with mutated flanking region on one side (except that crucial G nucleotide was conserved). These observations suggest that the central bases and certain flanking bases of one side of MARE can be altered without affecting much the binding affinity to MafG. Interestingly, $k_d$ are almost the same for MARE25, hOPSIN and hNQO1m MAREs, so the differences in $K_D$ values should be attributable solely to those in $k_a$. On the other hand, MafG only weakly bound to mGSTY MARE, hBglHS4 MARE or MARE23. The results of hBglHS4 MARE and MARE23 indicate that mutations in both flanking regions eliminated the binding of MafG. Inability of mGSTY MARE to bind MafG implies that simultaneous mutations on one side of flanking region and the other side of core region may also inhibit the binding of MafG homodimer to MARE.

### Comparison of $K_D$ values obtained from SPR imaging technique and from GMSA

In order to evaluate validity of the SPR imaging technique, the $K_D$ values obtained from the SPR binding analyses were compared to those from GMSA. The $K_D$ values determined by GMSA for MARE25, hOPSIN MARE and hNQO1m MARE were ranged in the magnitude of $10^{-7}$ (Fig. 5, lanes 1–7 and 15–28). MARE25, hOPSIN MARE and hNQO1m MARE showed high affinities, and the highest was MARE25. On the contrary, weak MafG binding to mGSTY MARE was observed, albeit it was not enough for the $K_D$ value determination (Fig. 5, lanes 29–35). No shifted bands were observed for MARE23 and hBglHS4 MARE (Fig. 5, lanes 8–14 and 36–42, respectively). These results are summarized in Table 3. Although $K_D$ values calculated from the SPR signals are ranged in the magnitude of $10^{-9}$, which are much smaller than those determined by GMSA, the comparative affinities obtained from these two distinct methods were very similar to each other. The affinity of MafG to MARE25 is the highest, and those to hOPSIN MARE and to hNQO1m MARE are intermediate. Interactions between MafG and mGSTY MARE, hBglHS4 MARE and MARE23 are not strong enough for the calculation of kinetic values.

## Discussion

In this study, we have developed an improved surface chemistry suitable for the SPR-based interaction study

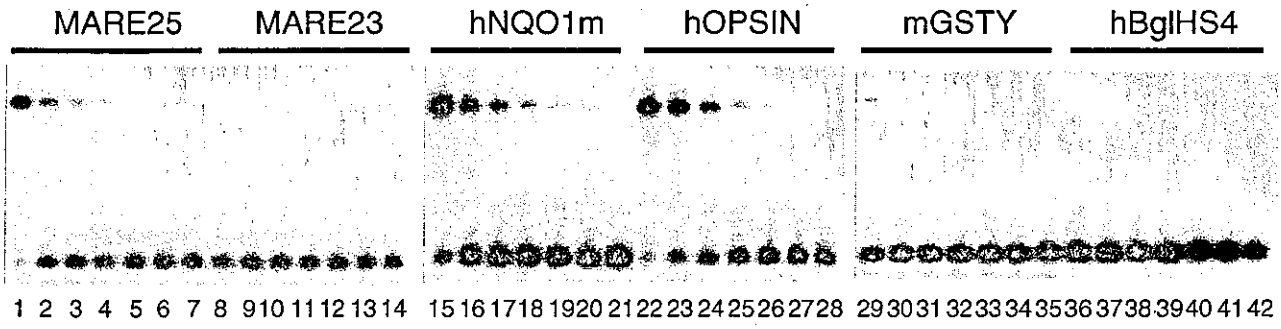


**Figure 5** Interaction between MafG and MARE-related sequences observed in GMSA. Six different probes were used for GMSA, MARE25 (lanes 1–7), MARE23 (lanes 8–14), hNQO1m (lanes 15–21), hOPSIN (lanes 22–28), mGSTY (lanes 29–35) and hBglHS4 (lanes 36–42). MafG homodimer concentrations are 360 nM (lanes 1, 8, 15, 22, 29, 36), 180 nM (lanes 2, 9, 16, 23, 30, 37), 90 nM (lanes 3, 10, 17, 24, 31, 38), 45 nM (lanes 4, 11, 18, 25, 32, 39), 22.5 nM (lanes 5, 12, 19, 26, 33, 40), 11.3 nM (lanes 6, 13, 20, 27, 34, 41) and 0 nM (lanes 7, 14, 21, 28, 35, 42).

of biomolecules on the chip. In order to overcome an inconvenience that immobilized DNAs are easily denatured upon exposure to organic solvent and reactive PEG, we first constructed the background by using PEG-thiol, and test molecules were attached on to the spots in the final step. This procedure allowed pre-annealed double-stranded DNAs to be immobilized on the chip in native form. Exploiting this procedure, we successfully fabricated a double-stranded DNA array on the chip. An SPR imaging analysis based on this procedure was performed to examine the specific interaction between MafG and several MARE-related motifs. The SPR imaging analyses gave the consistent results with those obtained from GMSA as far as the relative affinities are concerned, which in turn support our contention that the detected SPR signals reflect specific binding of MafG to MAREs. Thus, this study demonstrates that the double-stranded DNA array fabricated with the modified multistep procedure can be applied for the comprehensive analysis of the transcription factor-DNA interaction.

In the classic SPR studies on the DNA-protein interaction, biotin-streptavidin chemistry was usually adopted (Seimiya & Kurosawa 1996; Galio *et al.* 1997; Suzuki *et al.* 1998; Oda *et al.* 1999). In this case, biotin-terminated oligonucleotides are usually attached on streptavidin-modified surface. This method, however, has an inherent problem upon applying for the array fabrication, as cross-contamination among the spots may happen due to a strong and quick binding reaction between biotin and streptavidin. In order to perform a comprehensive quantification of binding affinities of transcription factors to various suboptimal sequences, it is a prerequisite to fabricate a double-stranded DNA array composed of multiple sequences that are very similar to one another. To this end, we adopted a method that allows immobilization of pre-annealed double-stranded DNAs on the chip, which can prevent mismatched hybridization and attain complete pairing between complementary DNAs. Indeed, we proved in this study that correct DNA immobilization was accomplished without contaminating spots in this procedure.

Another contrivance in this procedure is the choice of NHS-PEG-MAL as a heterobifunctional crosslinker. It should be noted that the interaction profiles between MafG and MAREs obtained with NHS-PEG-MAL-immobilized array show high level consistency with those observed in GMSA. This is in stark contrast to the results with SSMCC-immobilized array, as the latter results were not consistent with the GMSA data at all. We speculate that the flexible and hydrophilic linker provided by NHS-PEG-MAL might facilitate specific binding and prevent nonspecific adsorption of MafG by allowing the higher DNA mobility. We suppose that the PEG spacer should be generally effective to avoid nonspecific interactions of a test protein to the spot background regions. On the contrary, the salt concentration required for suppression of nonspecific binding must be determined for each protein.

Interactions between transcription factors and DNAs have been investigated by several methods including GMSA (Affolter *et al.* 1990; Yamamoto *et al.* 1990), filter-binding assay (Tanikawa *et al.* 1993) and SPR (Seimiya & Kurosawa 1996; Galio *et al.* 1997; Oda *et al.* 1999). The $K_D$ values, determined by these methods, are ranging from $10^{-7}$ to $10^{-10}$ and, especially, those obtained by SPR are from $10^{-7}$ to $10^{-9}$. One report compared $K_D$ values calculated by GMSA and SPR, and showed that the values are almost similar to one another ranged in the magnitude of $10^{-9}$ (Suzuki *et al.* 1998). In our case, $K_D$

values obtained by SPR ranged around $10^{-9}$, while those obtained by GMSA ranged around $10^{-7}$ (see Table 3). While the reason for this discrepancy is unclear at present, the following two differences in the measurement conditions may be pertinent.

First, DNA mobility is different from each other in the two measurements. Whereas DNAs are immobilized on a surface for SPR analysis, they are free in the solution in GMSA. Second, optimal salt concentrations are different from each other. Buffers with higher salt concentrations (more than 150 mM) are required for the SPR measurement to avoid the nonspecific adsorption of proteins on to the chip surface or immobilized DNA. On the contrary, GMSA buffer usually contains salts less than 75 mM, and nonspecific competitor DNA is typically added to the binding reaction solutions. In fact, we utilized in this study a high salt concentration (200 mM) to suppress nonspecific binding of DNA and MafG in the SPR analysis, whereas nonspecific DNA competitor was used for this purpose in GMSA. The kinetic profiles in the SPR measurement were investigated at various salt concentrations (Seimiya & Kurosawa 1996; Oda *et al.* 1999), and it was found that the lower salt concentration gives rise to the smaller $k_d$ values, and that $k_a$ values are usually not affected by the salt concentration. Consistent with the finding, we found that the dissociation of MafG and MARE25 became faster when sodium chloride concentration was as high as 450 mM (data not shown). Although these results do not explain the $K_D$ value difference between SPR and GMSA, we still consider that both SPR and GMSA measurements are valid for quantitative interaction analysis, since there is a very good correlation between the $K_D$ values of several MAREs obtained by SPR and GMSA.

All three small Maf family proteins are known to form either homodimer or heterodimer with other bZip superfamily members, including the CNC and Bach family members, and bind to MARE (Motohashi *et al.* 2002). These partner molecules cannot bind to MARE as a monomer or homodimer, so that small Mafs confer the DNA-binding ability on partner proteins and enable them to execute various activities directed by their functional domains through the heterodimerization. Since many of these Maf-based dimers exist in cells simultaneously, it seems very difficult to identify the primary Maf molecule or to evaluate the contribution of each dimer molecule to the gene regulation through a specific MARE in the regulatory region. One simple hypothesis is to assume that the most abundant dimer molecule in the nuclei may bind dominantly to MAREs, which leads to the notion that the balance between positive and negative regulators interacting to MAREs determines the eventual transcriptional activity. In fact, by adopting megakaryocytic gene regulation directed by NF-E2 p45 and small Maf proteins, we showed that quantitative alteration enables small Maf proteins to direct both active and repressive transcription (Motohashi *et al.* 2000). In the absence of small Mafs, p45 does not bind to DNA, so MARE-dependent transcription cannot be activated. In the excess of small Mafs, transcriptionally inactive small Maf homodimer occupies MAREs and represses the transcription. Only at the optimal concentration of p45 and small Maf, the maximum level of transcriptional activation is achieved by p45/small Maf heterodimer.

Recent data suggest that the qualitative difference may also be important for the interaction of MAREs and Maf-based dimers. When we examined *mafG::mafK* compound null mutant mice, mutant animals displayed quite selective MARE-dependent transcriptional abnormality (Katsuoka *et al.* 2003). In the mice, heme oxygenase-1 (HO-1) mRNA level was markedly increased. Similarly, Bach1-null mutant mice exhibit selective increase of HO-1 mRNA level (Sun *et al.* 2002). However, no apparent influence of small Maf decrease is observed for other MARE-dependent genes (our unpublished observation), indicating that small Maf and Bach1 make a major contribution to HO-1 gene regulation.

Considering this situation, comprehensive evaluations become crucial for Maf-based dimer interactions with various MARE-related sequences. In this regard, quite recently the interactions between various bZip superfamily proteins were investigated *in silico* with glass slide-based protein arrays and fluorescent-labelled protein probes (Newman & Keating 2003). We analysed in this study the DNA-protein interaction. Our system enables to examine all possible variations in MAREs quantitatively by using a couple of gold chips or more, since simultaneous detection of 96 samples is technically feasible on one chip. We adopted MafG homodimer as our initial trial of this SPR-array technology, since it is the simple system composed of a single molecule. Obviously, next important analysis will be comparing binding profiles of MafG homodimer, Bach1/small Maf heterodimer, and the other Maf-based heterodimer molecules on one chip. We surmise that Bach1/small Maf heterodimer may have the strongest preference toward HO-1 MAREs.

In spite of discrepancy in absolute $K_D$ values calculated from SPR and GMSA, there is a very good correlation between the two results in general. Since the SPR imaging is a powerful technique for the large-scale high-throughput analysis, we propose that the SPR imaging technique would be suitable for examining the general

binding preference of a transcription factor. We also propose that each specific interaction should be evaluated with the combination of multiple strategies, including SPR and GMSA for *in vitro* binding and reporter gene assay for *in vivo* binding.

## Experimental procedures

### Materials

The chemicals 8-amino-1-octanethiol, hydrochloride (8-AOT, Dojindo Laboratories), thiol terminated methoxypoly(ethylene glycol) MW 5000 (PEG-thiol, NOF), sulfosuccinimidyl-4-(*N*-maleimidomethyl)cyclohexane-1-carboxalate (SSMCC, Pierce), and *N*-hydroxysuccinimide-PEG maleimido MW 3400 (NHS-PEG-MAL, Shearwater), were all used as received.

### Preparation of oligonucleotide DNAs

The oligonucleotides for covalent immobilization on the surface were designed as 5′-HS-$(T)_{15}$-CGGAAT$(N)_{13}$TTACTC-3′, and synthesized at Hokkaido System Science or Sigma Genosys with the thiol group protected. The 15-base thymine stretch with a thiol group on the 5′-end was added to the test sequence, which is composed of 13 variable sequence flanked by 6 fixed bases on both sides. 5′- and 3′-fixed sequences were CGGAAT and TTACTC, respectively. Table 1 outlines the various sequences we used in this study. The thiol group on the 5′-end of the oligonucleotides were deprotected, and they were purified by gel filtration with NAP-5 Columns (Amersham Biosciences) as described by Sigma Genosys. The complementary oligonucleotides were synthesized against the variable region with 6-base fixed regions on both sides. The double-stranded DNAs were prepared by annealing longer and shorter complementary DNAs with and without 5′-thiol group, respectively. 25 μM of 5′-thiolated strand and 100 μM of its complementary strand were annealed in the 5× SSC solution (75 mM sodium citrate, 750 mM NaCl; pH 7.0). The solution was heated to 94 °C for 5 min, and quenched to 4 °C for 15 min, then incubated at 37 °C for 3 h, to complete the annealing.

### MafG protein preparation

MafG containing EHR and bZip motif, but lacking C-terminal 39 amino acids, was expressed in *Escherichia coli* as a $His_6$-tagged protein. The crude bacterial lysate was sequentially purified with SP sepharose (Pharmacia) and ProBond resin (Invitrogen). The recombinant protein was then cleaved with thrombin (Calbiochem) and further purified using SP sepharose. 200 μL of 125 nM MafG homodimer solution was used in one experiment.

### Fabrication of DNA arrays

The covalently immobilized DNA array with PEG background was obtained by the following procedure. Gold layer (45 nm) with thin chromium underlayer (3 nm) on SF10 glass slide (Schott) were used for SPR imaging measurement. The gold slide was immersed in a PEG-thiol solution (1 mM in 1 : 6 $H_2O$: Ethanol) for at least 3 h to form PEG layer on the surface. This slide was patterned at 40 mW/cm$^2$ for 2 h with chromium quartz mask, which had 96 square holes of 500 μm, by UV light source, which was generated from a 500 W super high-pressure mercury lamp (Ushio, Tokyo). After the surface was rinsed with water and ethanol, the slide was soaked in 1 mM ethanolic solution of 8-AOT for 1 h. This resulted in 96 amino-functionalized 500 μm squares with PEG background. Thiol-reactive maleimido-modified surface was created with 1 mM solution of heterobifunctional crosslinker SSMCC or NHS-PEG-MAL in phosphate buffer (20 mM phosphate; pH 7.0 and 100 mM NaCl). 10 nL drop of 10 μM 5′-thiol-terminated DNA in phosphate buffer was delivered automatically on the patterned surface by using an automated spotter (Toyobo, Osaka), and the reaction was carried out for overnight. Then the surface was rinsed with phosphate buffer and 5× SSC solution containing 0.1% SDS.

### SPR imaging analysis

The DNA array was placed immediately in the SPR imaging instrument (Toyobo). The SPR signals were obtained in the SPR buffer (20 mM HEPES (pH 7.9), 200 mM NaCl, 4 mM $MgCl_2$, 1 mM EDTA, and 100 μg/mL BSA). The SPR buffer and the sample in the same buffer were applied to the array surface with 100 μl/min. The SPR image and signal data were collected with MultiSPRinter Analysis program (Toyobo). The SPR difference image was constructed by using Scion Image (Scion, MD USA). The kinetic values were calculated with the program based on the simple reversible reaction model (George *et al.* 1995).

### Gel mobility shift assays

Gel mobility shift assays were performed as previously described (Kataoka *et al.* 1994a). The same oligonucleotides with those used in SPR detection, which are composed of a 13 bp-variable sequence flanked by 6 bp-fixed regions on both sides, were end labelled with γ-$^{32}$P-ATP for generating probes. MafG protein was incubated with probes in the gel shift buffer (20 mM HEPES (pH 7.9), 20 mM KCl, 5 mM dithiothreitol, 4 mM $MgCl_2$, 1 mM EDTA, 100 μg/mL BSA and 400 μg/mL poly(dIdC)) at 37 °C for 30 min. The resulting mixture was subjected to native polyacrylamide gel electrophoresis and visualized by autoradiography. The $K_D$ values were determined as described (Azam & Ishihama 1999) on the basis of the results obtained using protein concentration from 0 to 360 μM.

## Acknowledgements

We are grateful to Ms Kit Tong for critical reading of the manuscript. This work was supported by grants from ERATO (MY), the Ministry of Education, Culture, Sports, Science, and Technology (H.M. and M.Y.), the Ministry of Health, Labor and Welfare (M.Y.), CREST (H.M.), PROBRAIN (H.M.), and Special Coordination Fund for Promoting Science and Technology (H.M.).

## References


Affolter, M., Percival-Smith, A., Muller, M., Leupin, W. & Gehring, W.J. (1990) DNA binding properties of the purified Antennapedia homeodomain. *Proc. Natl. Acad. Sci. USA* **87**, 4093–4097.

Andrews, N.C., Erdjument-Bromage, H., Davidson, M.B., Tempst, P. & Orkin, S.H. (1993) Erythroid transcription factor NF-E2 is a haematopoietic-specific basic-leucine zipper protein. *Nature* **362**, 722–728.

Azam, T.A. & Ishihama, A. (1999) Twelve species of the nucleoid-associated protein from *Escherichia coli*. Sequence recognition specificity and DNA binding affinity. *J. Biol. Chem.* **274**, 33105–33113.

Boon, E.M., Salas, J.E. & Barton, J.K. (2002) An electrical probe of protein–DNA interactions on DNA-modified surfaces. *Nature Biotechn.* **20**, 282–286.

Brockman, J.M., Fruto, A.G. & Corn, R.M. (1999) A multi-step chemical modification procedure to create DNA arrays on gold surfaces for the study of protein–DNA interaction with surface plasmon resonance imaging. *J. Am. Chem. Soc.* **121**, 8044–8051.

Bulyk, M.L., Huang, X., Choo, Y. & Church, G.M. (2001) Exploring the DNA binding specificities of zinc fingers with DNA microarrays. *Proc. Natl. Acad. Sci. USA* **98**, 7158–7163.

Chan, J.Y., Han, X. & Kan, Y.W. (1993) Cloning of Nrf1, an NF-E2-related transcription factor, by genetic selection in yeast. *Proc. Natl. Acad. Sci. USA* **90**, 11371–11375.

Chidsey, C.E.D. & Loiacono, D.N. (1990) Chemical functionality in self-assembled monolayers: structural and electrochemical properties. *Langmuir* **6**, 682–691.

Dlakic, M., Grinberg, A.V., Leonard, D.A. & Kerppola, T.K. (2001) DNA sequence-dependent folding determines the divergence in binding specificities between Maf and other bZIP proteins. *EMBO J.* **20**, 828–840.

Fujiwara, K.T., Kataoka, K. & Nishizawa, M. (1993) Two new members of the *maf* oncogene family, *maf*K and *maf*F, encode nuclear b-Zip proteins lacking putative trans-activator domain. *Oncogene* **8**, 2371–2381.

Galio, L., Briquet, S., Cot, S., Guillet, J.G. & Vaquero, C. (1997) Analysis of interactions between huGATA-3 transcription factor and three GATA regulatory elements of HIV-1 long terminal repeat, by surface plasmon resonance. *Anal. Biochem.* **253**, 70–77.

George, A.J., French, R.R. & Glennie, M.J. (1995) Measurement of kinetic binding constants of a panel of anti-saporin antibodies using a resonant mirror biosensor. *J. Immunol. Methods* **183**, 51–63.

Huang, J., Dahlgren, D.A. & Hemminger, J.C. (1994) Photopatterning of self-assembled alkanethiolate monolayers on gold: a simple monolayer photoresist utilizing aqueous chemistry. *Langmuir* **10**, 626–628.

Itoh, K., Chiba, T., Takahashi, S., *et al.* (1997) An Nrf2/small Maf heterodimer mediates the induction of phase II detoxifying enzyme genes through antioxidant response elements. *Biochem. Biophys. Res. Commun.* **236**, 313–322.

Itoh, K., Igarashi, K., Hayashi, N., Nishizawa, M. & Yamamoto, M. (1995) Cloning and characterization of a novel erythroid cell-derived CNC family transcription factor heterodimerizing with the small Maf family proteins. *Mol. Cell. Biol.* **15**, 4184–4193.

Jordan, C.E. & Corn, R.M. (1997) Surface plasmon resonance imaging measurements of electrostatic biopolymer adsorption onto chemically modified gold surfaces. *Anal. Chem.* **69**, 1449–1456.

Jost, J.P., Munch, O. & Andersson, T. (1991) Study of protein–DNA interactions by surface plasmon resonance (real time kinetics). *Nucl. Acids Res.* **19**, 2788.

Kataoka, K., Fujiwara, K.T., Noda, M. & Nishizawa, M. (1994a) MafB, a new Maf family transcription activator that can associate with Maf and Fos but not with Jun. *Mol. Cell. Biol.* **14**, 7581–7591.

Kataoka, K., Igarashi, K., Itoh, K., *et al.* (1995) Small Maf proteins heterodimerize with Fos and potentially act as competitive repressors of NF-E2 transcription factor. *Mol. Cell. Biol.* **15**, 2180–2190.

Kataoka, K., Noda, M. & Nishizawa, M. (1994b) Maf nuclear oncoprotein recognizes sequences related to an AP-1 site and forms heterodimers with both Fos and Jun. *Mol. Cell. Biol.* **14**, 700–712.

Katsuoka, F., Motohashi, H., Tamagawa, Y., *et al.* (2003) Small Maf compound mutants display central nervous system neuronal degeneration, aberrant transcription, and Bach protein mislocalization coincident with myoclonus and abnormal startle response. *Mol. Cell. Biol.* **23**, 1163–1174.

Kerppola, T.K. & Curran, T.A. (1994) A conserved region adjacent to the basic domain is required for recognition of an extended DNA binding site by Maf/Nrl family proteins. *Oncogene* **9**, 3149–3158.

Kobayashi, A., Ito, E., Toki, T., *et al.* (1999) Molecular cloning and functional characterization of a new Cap'n'collar family transcription factor Nrf3. *J. Biol. Chem.* **274**, 6443–6452.

Kumar, R., Chen, S., Scheurer, D., *et al.* (1996) The bZIP transcription factor Nrl stimulates rhodopsin promoter activity in primary retinal cell cultures. *J. Biol. Chem.* **271**, 29612–29618.

Kusunoki, H., Motohashi, H., Katsuoka, F., Morohashi, A., Yamamoto, M. & Tanaka, T. (2002) Solution structure of the DNA-binding domain of MafG. *Nature Struct. Biol.* **9**, 252–256.

MacBeath, G. & Schreiber, S.L. (2000) Printing proteins as microarrays for high-throughput function determination. *Science* **289**, 1760–1763.

Moi, P., Chan, K., Asunis, I., Cao, A. & Kan, Y.W. (1994) Isolation of NF-E2-related factor 2 (Nrf2), a NF-E2-like basic leucine zipper transcriptional activator that binds to the tandem NF-E2/AP1 repeat of the beta-globin locus control region. *Proc. Natl. Acad. Sci. USA* **91**, 9926–9930.

Motohashi, H., Katsuoka, F., Shavit, J.A., Engel, J.D. & Yamamoto, M. (2000) Positive or negative MARE-dependent transcriptional regulation is determined by the abundance of small Maf proteins. *Cell* **103**, 865–875.

Motohashi, H., O'Connor, T., Katsuoka, F., Engel, J.D. & Yamamoto, M. (2002) Integration and diversity of the

regulatory network composed of Maf and CNC families of transcription factors. *Gene* **294**, 1–12.

Nelson, B.P., Frutos, A.G., Brockman, J.M. & Corn, R.M. (1999) Near-infrared surface plasmon resonance measurements of ultrathin films. 1. Angle shift and SPR imaging experiments. *Anal. Chem.* **71**, 3928–3934.

Newman, J.R. & Keating, A.E. (2003) Comprehensive identification of human bZIP interactions with coiled-coil arrays. *Science* **300**, 2097–2101.

Nishizawa, M., Kataoka, K., Goto, N., Fujiwara, K.T. & Kawai, S. (1989) v-maf, a viral oncogene that encodes a 'leucine zipper' motif. *Proc. Natl. Acad. Sci. USA* **86**, 7711–7715.

Oda, M., Furukawa, K., Sarai, A. & Nakamura, H. (1999) Kinetic analysis of DNA binding by the c-Myb DNA-binding domain using surface plasmon resonance. *FEBS Lett.* **454**, 288–292.

Ogino, H. & Yasuda, K. (1998) Induction of lens differentiation by activation of a bZIP transcription factor, L-Maf. *Science* **280**, 115–118.

Oyake, T., Itoh, K., Motohashi, H., *et al.* (1996) Bach proteins belong to a novel family of BTB-basic leucine zipper transcription factors that interact with MafK and regulate transcription through the NF-E2 site. *Mol. Cell. Biol.* **16**, 6083–6095.

Schena, M., Shalon, D., Davis, R.W. & Brown, P.O. (1995) Quantitative monitoring of gene expression patterns with a cDNA microarray. *Science* **270**, 467–470.

Seimiya, M. & Kurosawa, Y. (1996) Kinetics of binding of Antp homeodomain to DNA analyzed by measurements of surface plasmon resonance. *FEBS Lett.* **398**, 279–284.

Stamatoyannopoulos, J.A., Goodwin, A., Joyce, T. & Lowrey, C.H. (1995) NF-E2 and GATA binding motifs are required for the formation of DNase I hypersensitive site 4 of the human beta-globin locus control region. *EMBO J.* **14**, 106–116.

Sun, J., Hoshino, H., Takaku, K., *et al.* (2002) Hemoprotein Bach1 regulates enhancer availability of heme oxygenase-1 gene. *EMBO J.* **21**, 5216–5224.

Suzuki, F., Goto, M., Sawa, C., *et al.* (1998) Functional interaction of transcription factor human GA-binding protein subunits. *J. Biol. Chem.* **273**, 29302–29308.

Swaroop, A., Xu, J., Pawer, H., Jackson, A., Scolnick, C. & Agarwal, N. (1992) A conserved retina-specific gene encodes a basic motif/leucine zipper protein. *Proc. Natl. Acad. Sci. USA* **89**, 266–270.

Tanikawa, J., Yasukawa, T., Enari, M., *et al.* (1993) Recognition of specific DNA sequences by the c-myb protooncogene product: role of three repeat units in the DNA-binding domain. *Proc. Natl. Acad. Sci. USA* **90**, 9320–9324.

Tarlov, M.J., Burgess, D.R.F. & Gillen, J.G. (1993) UV photopatterning of alkanethiolate monolayers self-assembled on gold and silver. *J. Am. Chem. Soc.* **115**, 5305–5306.

Troughton, E.B., Bain, C.D., Whitesides, G.M., Nuzzo, R.G., Allara, D.L. & Porter, M.D. (1988) Monolayer films prepared by the spontaneous self-assembly of symmetrical and unsymmetrical dialkyl sulfides from solution onto gold substrates: structure, properties, and reactivity of constituent functional groups. *Langmuir* **4**, 365–385.

Venugopal, R. & Jaiswal, A.K. (1996) Nrf1 and Nrf2 positively and c-Fos and Fra1 negatively regulate the human antioxidant response element-mediated expression of NAD (P) H: quinone oxidoreductase1 gene. *Proc. Natl. Acad. Sci. USA* **93**, 14960–14965.

Yamamoto, M., Ko, L.J., Leonard, M.W., Beug, H., Orkin, S.H. & Engel, J.D. (1990) Activity and tissue-specific expression of the transcription factor NF-E1 [GATA] multigene family. *Genes Dev.* **4**, 1650–1662.

Zhu, H., Bilgin, M., Bangham, R., *et al.* (2001) Global analysis of protein activities using proteome chips. *Science* **293**, 2101–2105.

*Received*: 17 October 2003
*Accepted*: 26 November 2003

# Role of Nrf2 in the Regulation of CD36 and Stress Protein Expression in Murine Macrophages

## Activation by Oxidatively Modified LDL and 4-Hydroxynonenal

Tetsuro Ishii, Ken Itoh, Emilio Ruiz, David S. Leake, Hiroyuki Unoki, Masayuki Yamamoto, Giovanni E. Mann

*Abstract*—CD36 is an important scavenger receptor mediating uptake of oxidized low-density lipoproteins (oxLDLs) and plays a key role in foam cell formation and the pathogenesis of atherosclerosis. We report the first evidence that the transcription factor Nrf2 is expressed in vascular smooth muscle cells, and demonstrate that oxLDLs cause nuclear accumulation of Nrf2 in murine macrophages, resulting in the activation of genes encoding CD36 and the stress proteins A170, heme oxygenase-1 (HO-1), and peroxiredoxin I (Prx I). 4-Hydroxy-2-nonenal (HNE), derived from lipid peroxidation, was one of the most effective activators of Nrf2. Using Nrf2-deficient macrophages, we established that Nrf2 partially regulates CD36 expression in response to oxLDLs, HNE, or the electrophilic agent diethylmaleate. In murine aortic smooth muscle cells, expressing negligible levels of CD36, both moderately and highly oxidized LDL caused only limited Nrf2 translocation and negligible increases in A170, HO-1, and Prx I expression. However, treatment of smooth muscle cells with HNE significantly enhanced nuclear accumulation of Nrf2 and increased A170, HO-1, and Prx I protein levels. Because PPAR-γ can be activated by oxLDLs and controls expression of CD36 in macrophages, our results implicate Nrf2 as a second important transcription factor involved in the induction of the scavenger receptor CD36 and antioxidant stress genes in atherosclerosis. (***Circ Res.*** **2004;94:609-616.)**

**Key Words:** CD36 ■ Nrf2 ■ oxidized LDL ■ macrophages ■ vascular smooth muscle cells

Low-density lipoprotein (LDL) is susceptible to oxidative damage, and oxidatively modified LDL (oxLDL) plays a key role in the development of atherosclerotic lesions.[1,2] OxLDL is taken up via different scavenger receptors, and in macrophages, CD36, SR-A, and LOX-1 are the predominant receptors.[3–5] Enhanced formation of oxLDL in the vascular wall induces the formation of foam cells that accumulate cholesterol.[1–4] LDL oxidation is associated with the formation of a number of highly reactive molecules, such as lipid peroxides, lysophosphatidylcholine, oxysterols, and aldehydes,[6] which cause vascular inflammation and fibrosis[7,8] and expression of antiinflammatory genes in macrophages[9] and vascular smooth muscle cells.[10]

Components of oxLDL, such as 9-HODE and 13-HODE, activate peroxisome proliferator-activated receptor γ (PPAR-γ), resulting in the upregulation of the major oxLDL receptor CD36.[11] PPAR-γ appears to inhibit inflammatory response genes by antagonizing the activities of AP-1, NF-κB, and Stat 1 transcription factors.[12,13] Moreover, macrophages derived from mice in which the PPARγ gene has been "floxed out" fail to upregulate CD36 expression in response to treatment with thiazolidinedione drugs such as rosiglitazone.[14,15]

Our previous studies in vivo established that the transcription factor Nrf2, which interacts with electrophile (EpRE) and antioxidant (ARE) response elements and regulates expression of the detoxifying enzymes GST and NQO1 in tissues in response to dietary 2(3)-*t*-butyl-4-hydroxyanisole.[16] Moreover, the sensitivity to carcinogenesis is increased in Nrf2-deficient mice due to the loss of induction of ARE-regulated drug metabolizing enzymes and antioxidant genes,[17,18] and Nrf2 has also been implicated in the protection against oxidative damage induced by hyperoxia.[19] Thus, Nrf2 serves as a key transcription factor in the cytoprotection of tissues against electrophiles and reactive oxygen species.

We previously reported that Nrf2 regulates expression of HO-1, Prx I, anionic amino acid transporter xCT, and the ubiquitin/PKC-ζ–interacting protein A170 in murine peritoneal macrophages.[20] Activation of Nrf2 by electrophilic agents or reactive oxygen species is controlled by a

Original received March 19, 2003; resubmission received December 16, 2003; revised resubmission received January 14, 2004; accepted January 16, 2004.

From the Institutes of Community Medicine (T.I.) and Basic Medical Sciences (K.I., H.U., M.Y.), University of Tsukuba, Tsukuba, Japan; Cell and Molecular Biology Research Division (D.S.L.), School of Animal and Microbial Sciences, University of Reading, UK; Centre for Cardiovascular Biology and Medicine (E.R., G.E.M.), GKT School of Biomedical Sciences, King's College London, Guy's Campus, London, UK.

Correspondence to Prof Tetsuro Ishii, Institute of Community Medicine, University of Tsukuba, Tsukuba 305-8575, Japan. E-mail teishii@md.tsukuba.ac.jp and Prof Giovanni E. Mann, Centre for Cardiovascular Biology and Medicine, GKT School of Biomedical Sciences, King's College London, Guy's Campus, London SE1 1UL, UK. E-mail giovanni.mann@kcl.ac.uk



*Circulation Research* is available at http://www.circresaha.org

DOI: 10.1161/01.RES.0000119171.44657.45

novel cytoplasmic protein designated Keap 1 that interacts with Nrf2 and negatively regulates nuclear translocation of Nrf2 and facilitates degradation of Nrf2 via the proteasome.[21,22]

OxLDLs upregulate HO-1 and Prx I expression in murine macrophages[11] and porcine aortic smooth muscle cells,[23] whereas immunostaining and in situ hybridization have established that HO-1 is prominently expressed in the endothelium and foam cells/macrophages in the intima of atherosclerotic lesions in humans and mice.[24] HO-1 plays an essential antiinflammatory role in vitro and in vivo,[25] and Prx I due its thioredoxin peroxidase activity can reduce hydrogen peroxide[26] and modulate $H_2O_2$-mediated activation of NF-κB.[27]

We have investigated the role of Nrf2 in the induction of stress proteins by oxLDLs and 4-hydroxynonenal (HNE) in murine peritoneal macrophages and aortic smooth muscle cells (SMCs) isolated from wild-type and *nrf2*-knockout mice. We show for the first time that oxLDLs activate Nrf2 in murine macrophages, but less efficiently in SMCs, and that HNE, one of the major end products of lipid oxidation and contained in oxLDL, is a potent activator of Nrf2 translocation to the nucleus in both cell types. Moreover, we provide novel evidence that Nrf2 is an important regulator of CD36 expression in murine macrophages. Because PPAR-γ can be activated by oxLDLs and controls expression of CD36 in macrophages, our results implicate Nrf2 as an additional transcription factor involved in the regulation oxLDL uptake by the vascular wall and induction of antioxidant stress genes in atherosclerosis.

## Materials and Methods

### Reagents

4-Hydroxy-2-nonenal (HNE) and 15-deoxy-$\Delta^{12,14}$-$PGJ_2$ (15d-$PGJ_2$) were from Calbiochem, rosiglitazone was from Cayman Chemical, HPODE was from Biomol, monoclonal antibody reactive with murine CD36 was from Cascade Biosciences, and Dr Western (marker for Western blot) was from Oriental Yeast Co. Ltd. All other chemicals, actin antibody (A-2066), lysophosphatidylcholine (LPC), 7-ketocholesterol, hexanal, malondialdehyde, and 7β-hydroxycholesterol were from Sigma Chemical Co.

### Culture of Mouse Peritoneal Macrophages and Aortic Smooth Muscle Cells

Mouse peritoneal macrophages were prepared from female ICR mice and *nrf2*-knockout mice backcrossed with ICR mice that 4 days previously received an intraperitoneal injection of 2 mL of 4% thioglycollate broth.[20] Additional experiments were performed using peritoneal macrophages from *CD36*-deficient female mice. Macrophages were maintained in RPMI 1640 medium (10% fetal calf serum), chemical agents added and cultured as indicated. Explant cultures of mouse aortic smooth muscle cells (SMCs) were maintained in Dulbecco's modified Eagle's medium (10% fetal calf serum), and experiments conducted with passage 5 to 10 cells. Animal experimental procedures were in accordance with University of Tsukuba's Regulations on Animal Experiments and Japanese Governmental Law No. 105.

### Preparation of LDL

LDL was isolated from normal human blood by ultracentrifugation in the presence of EDTA as described previously.[10] Oxidatively modified LDLs were formed by incubating LDL with 5 μmol/L $CuSO_4$ at 37°C, and the conjugated diene content determined by measuring absorbance at 234 nm. Lipid hydroperoxides in native (nLDL), moderately oxidized LDL (moxLDL), and highly oxidized LDL (oxLDL) were 40, 64, and 80 nmol/mg protein, respectively, and the relative electrophoretic mobilities of moxLDL and oxLDL (compared with native LDL) were 1.3 and 4.6, respectively.

### Western Blot Analysis

Before electrophoresis, a marker dye and 2-mercaptoethanol were added to lysates, which were then fractionated by SDS-polyacrylamide gel electrophoresis and electrotransferred onto an Immobilon membrane (Millipore).[20] Polyclonal rabbit antisera raised against purified rat HO-1, rat Prx I, and recombinant mouse A170 and Nrf2 were used. Nuclear pellets were prepared after cell lysis in 0.5% Nonidet P-40 containing buffer.[20] Densitometric analysis was performed using NIH Image software.

### Northern Blot Analysis

Total RNA was extracted from cells using RNeasy (QIAGEN), fractionated by electrophoresis and transferred to Zeta-Probe GT membranes (Bio-Rad). Membranes were probed with [$^{32}$P]-labeled cDNA prepared by Megaprime labeling (Amersham), using 18S rRNA cDNA as an internal control. As described previously,[21] cDNA fragments for A170, HO-1, Prx I, and CD36 were prepared from Bluescript plasmid and used for hybridization.

### Reverse Transcription–PCR Analysis

Oligonucleotide primers used for RT-PCR were as follows: 5′-TGTGCTAGACATTGGCAAATG-3′ and 5′-CTTCTCCTAAAGATAGGTGTG-3′ for detecting mouse CD36 mRNA, 5′-AAAGATAGACACCATCACCC-3′ and 5′-GCGACAGTCAAAAGTCTTCTC-3′ for mouse LOX-1 mRNA, 5′-TCTCTACCTCCTTGTGTTTG-3′ and 5′-GATTGCATCCAGTGAATTCC-3′ for mouse macrophage scavenger receptor I (SR-A) mRNA, and 5′-TGAAGGTCGGAGTCAACGGATTTGGT-3′ and 5′-CATGTGGGCCATGAGGTCCACCAC-3′ for mouse GAPDH mRNA. Total RNAs isolated from macrophages treated with moxLDL or oxLDL for 24 hours were analyzed by RT-PCR using a QIAGEN OneStep RT-PCR kit. An aliquot of each RT-PCR mixture was electrophoresed on a 1.2% agarose gel and stained with Vistra Green (Amersham Pharmacia Biotech). The signal intensity of the RT-PCR products was determined using Fluoroimager 595 (Amersham Pharmacia Biotech). The amounts of total RNA templates and cycle numbers for amplification were chosen in quantitative ranges determined by plotting signal intensities as functions of the template amounts and cycle numbers. Nucleotide sequences of the RT-PCR products were verified.

### Oil Red O Staining

Mouse peritoneal macrophages were incubated for 24 hours at 37°C in 5% $CO_2$ in RPMI 1640 medium containing 10% FCS in the absence or presence of HNE (10 μmol/L) or moxLDL or oxLDL (200 μg protein $mL^{-1}$). Macrophages were washed twice, fixed in formalin, and stained with oil red O. The area of lipid-loaded macrophages was measured using a computerized MacSCOPE image analysis system (Mitani Corp).

## Results

### Oxidatively Modified LDL Activates Nrf2 in Peritoneal Macrophages

The effects of oxLDLs on nuclear accumulation of Nrf2 and stress gene expression in murine macrophages are shown in Figure 1. Cells were pretreated for 5 hours with nLDL, moxLDL, and oxLDL, and nuclear fractions were analyzed by immunostaining. Nuclear levels of Nrf2 were enhanced markedly after treatment with either moxLDL or oxLDL, whereas nLDL increased Nrf2 translocation marginally (Fig-

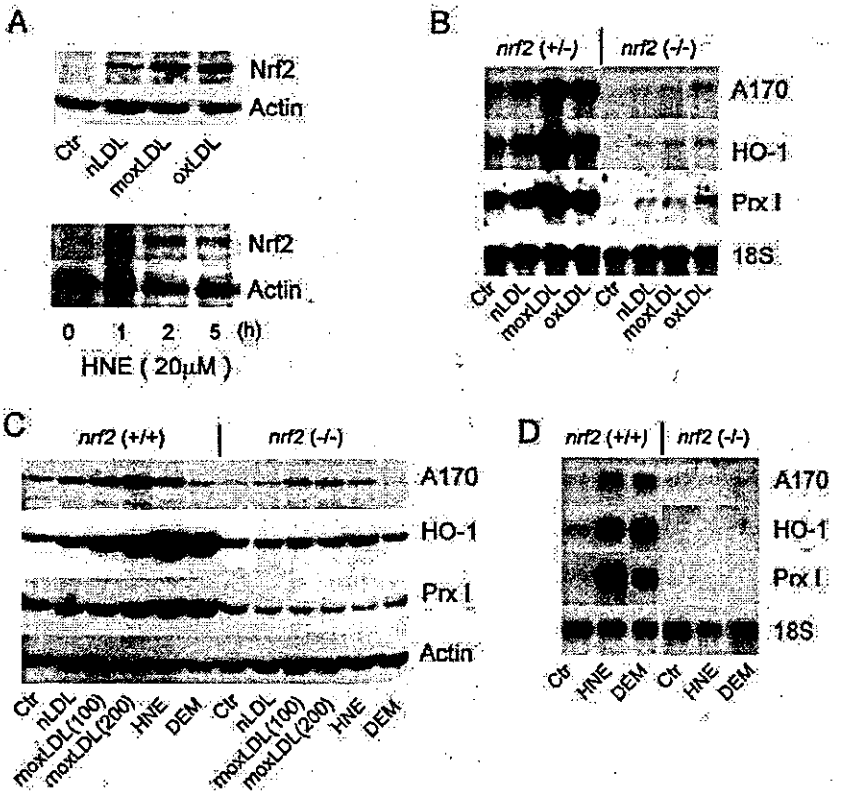


**Figure 1.** OxLDL and HNE induced nuclear accumulation of Nrf2 and A170, HO-1, and Prx I expression in peritoneal macrophages. A, Nrf2 and actin (internal control) in nuclear fractions were detected by immunoblot analysis. Top, Cells were incubated for 5 hours in the absence (Ctr) or presence of 100 μg protein $mL^{-1}$ native LDL (nLDL), moderately oxidized LDL (moxLDL), or highly oxidized LDL (oxLDL). Bottom, Time-dependent nuclear accumulation of Nrf2 in cells treated with 20 μmol/L HNE. Nuclear fractions were prepared from control (0 hours) and HNE-treated (1 to 5 hours) wild-type cells. B, Nrf2-dependent upregulation of A170, HO-1, and Prx I mRNA (5 hours) by 250 μg protein $mL^{-1}$ nLDL, moxLDL, and oxLDL in *nrf2*$^{+/-}$ and *nrf2*$^{-/-}$ cells. Ribosomal 18S RNA was used as an internal control. C, A170, HO-1, Prx I, and actin (internal control) protein expression in *nrf2*$^{+/+}$ and *nrf2*$^{-/-}$ macrophages incubated for 8 hours in the absence (Ctr) or presence of nLDL (100 μg protein $mL^{-1}$) or moxLDL (100 or 200 μg protein $mL^{-1}$), HNE (20 μmol/L), or diethylmaleate (100 μmol/L). D, Nrf2-dependent upregulation of A170, HO-1, and Prx I mRNA levels in cells treated for 5 hours with either 20 μmol/L HNE or 100 μmol/L DEM.

ure 1A, top). Increased Nrf2 levels induced by these agents were also detected in whole cell lysates (data not shown).

When effects of oxLDLs (5 hours) on A170, HO-1, and Prx I mRNA levels were determined in heterozygous mutant and Nrf2-deficient (homozygous mutant) macrophages, both moxLDL and oxLDL increased A170, HO-1, and Prx I mRNA levels (relative to 18S rRNA) in *nrf2*$^{+/-}$ cells, whereas nLDL had a negligible effect (Figure 1B). Basal expression of these transcripts was significantly lower in *nrf2*$^{-/-}$ compared *nrf2*$^{+/-}$ (or wild type, data not shown) macrophages, and oxLDLs caused only marginal increases in mRNA levels (Figure 1B). moxLDL only caused a concentration-dependent increase in A170, HO-1, and Prx I expression in *nrf2*$^{+/+}$ macrophages. In *nrf2*$^{-/-}$ cells, moxLDL only slightly enhanced A170 levels but did not increase expression of either HO-1 or Prx I (Figure 1C).

## Effects of LDL Components on Induction of Stress Proteins

Because oxidized LDL contains lipid hydroperoxides, oxysterols, and aldehydes,[1,6,28] we examined the effects of lysophosphatidylcholine (LPC), HPODE, 7-ketocholesterol, hexanal, malondialdehyde, 7β-hydroxycholesterol, and 4-hydroxy-2-nonenal (HNE). Treatment of macrophages for 8 hours with either LPC (50 μmol/L), 7-ketocholesterol (20 and 40 μmol/L), or hexanal (250 and 500 μmol/L) had no significant effect on A170, HO-1, and Prx I expression, whereas HPODE or malondialdehyde only slightly enhanced protein levels at 50 μmol/L (data not shown). 7β-Hydroxycholesterol increased A170, HO-1, and Prx I expression only at concentrations above 50 μmol/L (data not shown). We found that HNE was the most effective activator of Nrf2-mediated increases in stress protein mRNA and protein levels (Figures 1C and 1D). The estimated content of HNE in highly oxidized LDL is 114 nmol/mg LDL protein,[6] corresponding to ≈17 μmol/L HNE when 150 μg protein $mL^{-1}$ oxidized LDLs were added to culture media. These results suggest that HNE contained in oxidized LDL could be one of the activators of Nrf2.

## 4-Hydroxynonenal Activates Nrf2 and Stress Protein Expression in Peritoneal Macrophages

HNE increased nuclear translocation of Nrf2 after 1 to 5 hours (Figure 1A, bottom). HNE and diethylmaleate (DEM), a typical Nrf2-activating electrophilic agent,[20] increased stress protein expression in *nrf2*$^{+/+}$ macrophages, with responses markedly attenuated in *nrf2*$^{-/-}$ cells (Figures 1C and 1D).

## Effects of Oxidatively Modified LDL and HNE in Murine Aortic Smooth Muscle Cells

In contrast to our findings in macrophages, oxLDLs had a negligible effect on nuclear translocation and accumulation of Nrf2 in murine aortic smooth muscle cells (SMCs) (Figure 2A, top). In contrast, a rapid (1 to 3 hours), transient increase in nuclear Nrf2 levels was observed in SMCs treated with HNE (Figure 2A, bottom). When the effects of oxLDLs, HNE, and DEM on transcriptional activation of A170, HO-1, and Prx I were examined in *nrf2*$^{+/+}$ SMCs under standard culture conditions, relatively

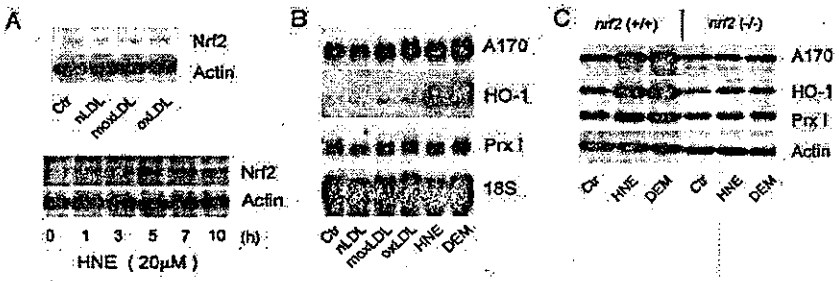


**Figure 2.** Activation of Nrf2 and enhanced expression of A170, HO-1, and Prx I in murine aortic smooth muscle cells. A, Nrf2 and actin (internal control) in nuclear fractions were detected by immunoblot analysis. Top, Cells were treated for 5 hours in the absence (Ctr) or presence of 100 μg protein $mL^{-1}$ nLDL, moxLDL, oxLDL. Bottom, Time-dependent nuclear accumulation of Nrf2 in SMCs treated with 20 μmol/L HNE. Nuclear fractions were prepared from *nrf2*$^{+/+}$control (0 hours) and HNE-treated (1 to 10 hours) SMCs. B, A170, HO-1, and Prx I mRNA levels in SMCs treated for 5 hours with 100 μg protein $mL^{-1}$ nLDL, moxLDL, and oxLDL, 20 μmol/L HNE, or 100 μmol/L DEM. C, Immunoblot showing A170, HO-1, and Prx I expression in *nrf2*$^{+/+}$ and *nrf2*$^{-/-}$ SMCs treated for 8 hours with 20 μmol/L HNE or 100 μmol/L DEM.

high basal mRNA levels were detected for Prx I and A170, whereas basal HO-1 mRNA levels were low (Figure 2B). Notably, nLDL, moxLDL, and oxLDL failed to increase mRNA (Figure 2B) or protein (data not shown) levels for A170, HO-1, and Prx I in *nrf2*$^{+/+}$ SMCs.

HNE and DEM significantly increased mRNA and protein levels of A170 and HO-1 in *nrf2*$^{+/+}$ SMCs, whereas Prx I expression was only slightly enhanced (Figures 2B and 2C). In *nrf2*$^{-/-}$ SMCs, neither HNE nor DEM affected A170, HO-1, and Prx I expression (Figure 2C). Thus, as in macrophages, increased stress protein expression in SMCs induced by HNE or DEM is largely dependent on activation of Nrf2, establishing a strong correlation between nuclear accumulation of Nrf2 and transcriptional activation of stress genes.

## Activation of CD36 Gene Expression by HNE and DEM in Murine Peritoneal Macrophages

CD36 is the major scavenger receptor for the uptake of oxidatively modified LDL in macrophages.[3–5,29,30] We previously isolated the mouse homologue of a CD36 cDNA clone,[31] and in the present study, Northern blot analysis showed that HNE and DEM increased CD36 mRNA levels in *nrf2*$^{+/+}$ but not *nrf2*$^{-/-}$ macrophages (Figure 3A, top). Immunoblot experiments established that HNE and DEM (8 hours) caused a 2.2-fold and 1.4-fold increase in CD36 protein levels in *nrf2*$^{+/+}$ macrophages, whereas upregulation of CD36 was minimal in *nrf2*$^{-/-}$ cells (Figure 3A, bottom). These findings suggest that increased CD36 expression in response to HNE and DEM is largely dependent on the activation of Nrf2. As basal expression of CD36 in *nrf2*$^{+/+}$ and *nrf2*$^{-/-}$ macrophages was similar (Figure 3A, bottom), this suggests that Nrf2 does not modulate basal CD36 expression.

## Nrf2-Dependent Upregulation of CD36 Expression by Oxidatively Modified LDL

We could not detect upregulation of CD36 protein levels in macrophages treated with moxLDL or oxLDL for 8 hours (Figure 3A, bottom), and therefore examined concentration-

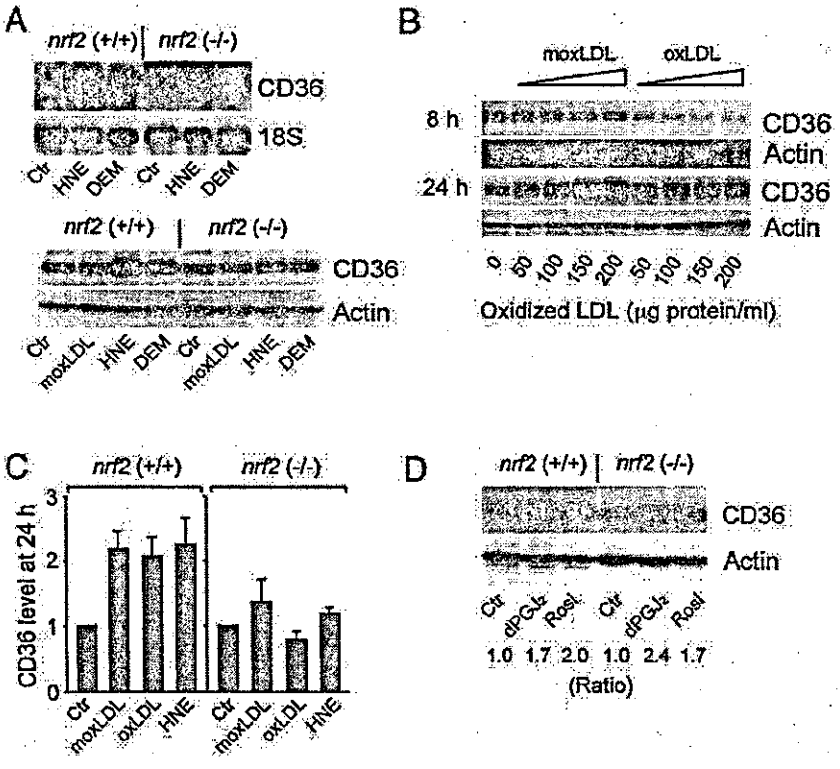


**Figure 3.** Nrf2-dependent induction of CD36 expression in murine peritoneal macrophages. A, Top, CD36 mRNA levels in *nrf2*$^{+/+}$ and *nrf2*$^{-/-}$ macrophages treated for 5 hours with 20 μmol/L HNE or 100 μmol/L DEM. Bottom, Immunoblot comparing CD36 protein levels in *nrf2*$^{+/+}$ and *nrf2*$^{-/-}$ macrophages treated for 8 hours with 100 μg protein $mL^{-1}$ moxLDL, 20 μmol/L HNE, or 100 μmol/L DEM. B, Immunoblot showing CD36 expression in *nrf2*$^{+/+}$ macrophages treated either for 8 or 24 hours in the absence (Ctr) or presence of 50 to 200 μg protein $mL^{-1}$ moxLDL or oxLDL. C, Densitometric analysis of 24-hour treatment with moxLDL, oxLDL, or HNE (20 μmol/L) on CD36 expression in *nrf2*$^{+/+}$ and *nrf2*$^{-/-}$ macrophages. Values denote mean±SEM of experiments in 3 to 5 different cell cultures. D, Effects of PPARγ activators on CD36 protein levels in *nrf2*$^{+/+}$ and *nrf2*$^{-/-}$ macrophages. Cells were treated for 24 hours in the absence (Ctr) or presence of 5 μmol/L 15d-prostaglandin $J_2$ (dPGJ$_2$) or 5 μmol/L rosiglitazone (Rosi).

dependent effects of moxLDL and oxLDL (50 to 200 μg protein $mL^{-1}$) on CD36 expression at 8 and 24 hours in $nrf2^{+/+}$ macrophages. moxLDL and oxLDL dose-dependently increased CD36 levels only after 24 hours (Figure 3B). When effects of moxLDL and oxLDL (200 μg protein $mL^{-1}$, 24 hours) were compared in $nrf2^{+/+}$ and $nrf2^{-/-}$ macrophages, induction of CD36 was significantly attenuated in Nrf2-deficient macrophages (Figure 3C). HNE markedly increased CD36 levels in $nrf2^{+/+}$ macrophages but was less effective in $nrf2^{-/-}$ macrophages, providing the first direct evidence that Nrf2 is important in the activation of CD36 gene expression in macrophages exposed to oxLDLs or HNE.

Similar experiments with SMCs failed to detect CD36 mRNA and protein expression under basal conditions or after treatment with 100 μg protein $mL^{-1}$ nLDL, moxLDL or oxLDL, HNE (20 μmol/L, 5 to 8 hours), or DEM (100 μmol/L, 5 to 8 hours) (data not shown).

### PPAR-γ Activators Upregulate CD36 Expression in Nrf2-Deficient Macrophages

PPAR-γ plays an important role in the induction of CD36 by oxLDLs.[11,32,33] Under our experimental conditions, CD36 expression was upregulated in $nrf2^{+/+}$ and $nrf2^{-/-}$ macrophages by the PPAR-γ activators 15d-$PGJ_2$ and rosiglitazone (Figure 3D), indicating that PPAR-γ activation of CD36 gene expression occurs via a signaling pathway distinct from Nrf2.

### Effects of Oxidatively Modified LDL on Expression of Other Scavenger Receptors

We used quantitative RT-PCR to compare CD36, LOX-1, and SR-A mRNA levels in murine macrophages. In contrast to upregulation of CD36 in response to moxLDL and oxLDL (Figure 4A), mRNA levels for LOX-1 were downregulated whereas levels for SR-A remained unchanged (data not shown). Our findings are consistent with a previous report that increased uptake of oxLDL in monocytes is the result of increased expression of CD36 but not of the scavenger receptor SR-A type I or type II.[34] Oil red O staining of macrophages revealed that moxLDL significantly enhanced the accumulation of cholesterol in $nrf2^{+/+}$ cells, whereas the intensity of staining was much lower in Nrf2-deficient cells (see Figures 4B and 4C). HNE alone only slightly enhanced oil red O staining in both cell types. These results indicate that Nrf2-dependent upregulation of CD36 leads to an accumulation of cholesterol in macrophages treated with moderately oxidized LDL. However, experiments with $CD36^{-/-}$ peritoneal macrophages revealed that CD36 is not essential for activation of Nrf2 by oxLDL or HNE (data not shown).

## Discussion

We report the first evidence that oxLDLs and HNE induce nuclear translocation of Nrf2 in murine peritoneal macrophages, resulting in an upregulation of the scavenger receptor CD36 and antioxidant stress proteins A170, HO-1, and Prx I. Our study establishes (1) Nrf2 as a novel signaling pathway involved in the regulation of CD36 gene expression in macrophages, (2) HNE as a potent activator of Nrf2 in both macrophages and SMCs, and (3) oxLDLs as effective activators of Nrf2 in macrophages but not in SMCs expressing negligible levels of CD36. In addition to identifying Nrf2 as a key transcription factor controlling antioxidant gene expression, our findings implicate Nrf2 as an important signaling pathway in atherosclerosis.

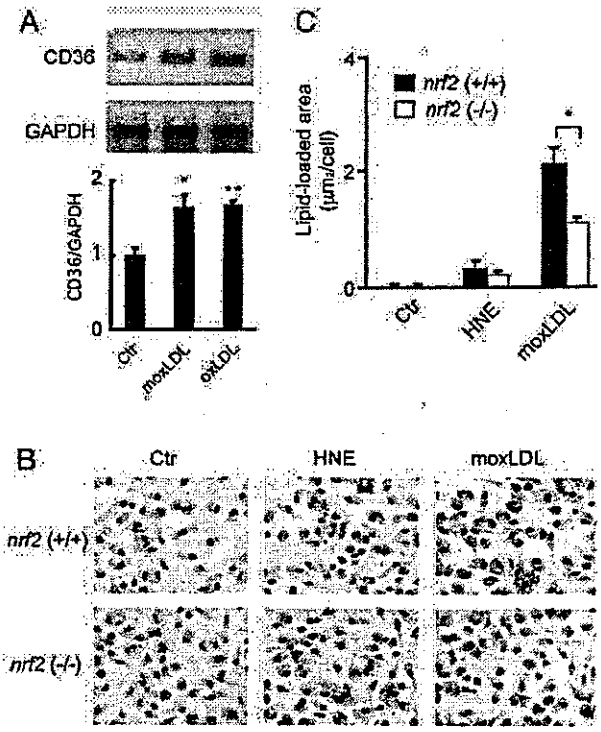


**Figure 4.** Effects of oxLDLs and HNE on CD36 expression and cholesterol accumulation in peritoneal macrophages. A, RT-PCR analysis of CD36 gene expression in cells treated for 24 hours in the absence (Ctr) or presence of 200 μg protein $mL^{-1}$ moxLDL or oxLDL, using GAPDH mRNA as a loading control. B, Oil red O staining of $nrf2^{+/+}$ and $nrf2^{-/-}$ macrophages treated for 24 hours in the absence (Ctr) or presence of 10 μmol/L HNE or 200 μg protein $mL^{-1}$ moxLDL. C, Lipid-loaded area of ~150 to 200 macrophages measured by oil red O staining. Values denote mean±SEM of measurements in 3 different experiments. $^{*}P<0.05$, $^{**}P<0.01$.

In macrophages, CD36 can be upregulated by oxLDL,[29,30] and previous studies have established an integral role for PPAR-γ in CD36 gene expression.[11,32] PPAR-γ modulates lipid homeostasis and antiinflammatory responses in macrophages[33] and is expressed at high levels in foam cells in atherosclerotic lesions.[11,35] PPAR-γ–deficient macrophages express low levels of both CD36 mRNA and protein, suggesting that PPAR-γ controls basal levels of CD36.[15] However, the latter study did not examine whether oxLDLs enhance CD36 expression in PPAR-γ–deficient macrophages. We have identified Nrf2 as a novel signaling pathway, distinct from PPAR-γ, that also upregulates CD36 expression in macrophages treated with oxLDLs. The following evidence supports this conclusion. First, HNE readily enters cells and is highly reactive with proteins and metabolized by enzymes such as aldo-keto-reductase.[28] Second, HNE does not activate

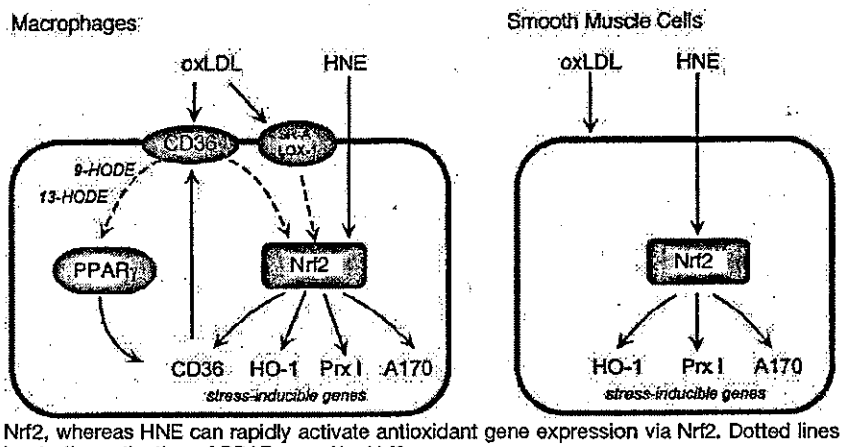


**Figure 5.** Nrf2-dependent activation of CD36 and antioxidant stress genes in murine peritoneal macrophages by oxidatively modified LDL (eg, moxLDL or oxLDL) or HNE. Activation of the Nrf2 pathway in macrophages leads to an upregulation of CD36 expression and uptake of oxidatively modified LDL. HNE, one of the end products of lipid peroxidation, induces rapid activation (2 to 5 hours) of Nrf2 and enhanced expression of HO-1, Prx I, and A170. Induction of antioxidant stress genes via Nrf2 affords protection of cells against the toxicity of oxLDLs. In murine aortic smooth muscle cells, expressing low levels of oxLDL scavenger receptors, oxidatively modified LDLs cause a negligible activation of Nrf2, whereas HNE can rapidly activate antioxidant gene expression via Nrf2. Dotted lines denote intracellular signaling cascades leading to the activation of PPAR-γ and/or Nrf2.

PPAR-γ directly,[11,34] whereas rapid activation of Nrf2 by HNE leads to CD36 gene expression in macrophages (Figures 3A and 3C), implicating Nrf2 as an important transcription factor in the upregulation of CD36 in oxidative stress. Third, as PPAR-γ activators 15d-$PGJ_2$ and rosiglitazone increased CD36 protein levels in both *nrf2*$^{+/+}$ and *nrf2*$^{-/-}$ macrophages (Figure 3D), this suggests that activation of PPAR-γ can occur in the absence of Nrf2.

HNE proved to be one of the most effective activators of Nrf2; however, we cannot exclude the possibility that other components of oxLDL may also have led to Nrf2 activation. Recent studies indicate that oxidized choline glycerophospholipid in oxLDL influences the binding of oxLDL to CD36.[36,37] Earlier studies from this group provided convincing evidence that lipid accumulation and foam cell formation were significantly reduced in *CD36*$^{-/-}$ mice.[38] Our preliminary studies with *CD36*$^{-/-}$ mice established that oxLDL and HNE induced activation of Nrf2 in murine macrophages is not dependent on CD36 (data not shown).

Kavanagh et al[39] reported that CD36 and PPAR-γ are differentially expressed in human monocytes in response to LDL oxidized to different degrees. Using oxLDL preparations similar to those in our study, this group established that moxLDL, but not oxLDL, enhanced DNA binding to PPAR-γ. Our experiments with *nrf2*$^{-/-}$ macrophages revealed that moxLDL still appears to increase, although not significantly, CD36 expression, whereas responses to oxLDL and HNE were abrogated (Figure 3C). We believe that HNE selectively activates Nrf2, resulting in a PPAR-γ–independent expression of CD36 in macrophages. In this context, HNE has been detected in rabbit and human atherosclerotic lesions,[40,41] and Napoli et al[42] reported that a large percentage of all fetal aortic atherogenic sites contained malondialdehyde-lysine and HNE-lysine epitopes.

Our findings in *nrf2*$^{+/+}$ macrophages indicate that moxLDL and oxLDL selectively upregulate CD36 mRNA expression (Figure 4A) but not the scavenger receptors LOX-1 or SR-A (data not shown). In contrast, in *nrf2*$^{-/-}$ macrophages oxLDLs and HNE fail to significantly increase CD36 levels (Figure 3C). We found multiple ARE-like sequences in the promotor region of murine CD36-encoding gene (GenBank accession No. AF434766) and further studies are required to identify the functional Nrf2-interacting ARE in this promotor region. A recent study indicates that AREs play a direct role in mediating the induction of glutathione synthesis by oxLDL, suggesting a role of Nrf2 in this response.[43] The lack of induction of CD36 in *nrf2*$^{-/-}$ macrophages was associated with a reduced accumulation of cholesterol (Figures 4B and 4C), indicating that the Nrf2 signaling pathway plays a key role in mediating oxLDL uptake via CD36. Although there are limited reports that human cultured aortic SMCs express CD36,[44–46] we could not detect CD36 expression in SMCs cultured from either *nrf2*$^{+/+}$ and *nrf2*$^{-/-}$ mice (data not shown). These differences in CD36 expression may be important for comparisons of human and murine models of atherosclerosis.

Our study provides the first evidence that Nrf2, in addition to coordinating cellular defenses against electrophilic agents and reactive oxygen species, also plays an essential role in regulating CD36 expression. Figure 5 summarizes our experimental findings, and highlights that in murine macrophages oxLDLs and HNE lead to a rapid nuclear accumulation of Nrf2 and subsequent induction of CD36 and the stress proteins A170, HO-1, and Prx I. In murine SMCs, oxLDLs fail to induce nuclear translocation of Nrf2 and gene activation of CD36 and stress proteins most likely due to the fact that murine SMCs express low levels of scavenger receptors. In *nrf2*$^{-/-}$ macrophages, oxLDLs could still signal via PPAR-γ, whereas the Nfr2-dependent induction of antioxidant stress proteins is markedly attenuated. The recent report that PPAR-γ inhibits Nrf2-induced expression of the gene encoding thromboxane synthase in macrophages,[47] suggests that the transcriptional regulators PPAR-γ and Nrf2 may interact functionally to modulate CD36 gene expression.

Future studies in vivo, using wild-type and Nrf2-deficient mice, should enable us to determine whether Nrf2 is expressed in atherosclerotic lesions, and whether this transcription factor modulates the progression of foam cell formation and atherosclerosis. Because Nrf2 has been implicated as a regulator of HO-1 expression and HO-1 mRNA and protein levels are increased in human atherosclerotic lesions,[29] it seems likely that Nrf2 plays a role in atherogenesis. Identi-

fying the intracellular signaling pathways modulating Nrf2 and PPAR-γ will provide important insights into their role in regulating vascular gene expression[48] and may provide a basis for the design of therapeutic strategies to treat atherosclerosis.

## Acknowledgments

This work was supported by the Japan Society for the Promotion of Science, University of Tsukuba Research Projects, and a Wellcome Trust Short-Term Collaborative Travel Grant (T. I., G.E.M.). We thank Dr S. Taketani (Kansai Medical University, Moriguchi, Osaka, Japan) for providing the anti–HO-1 antibody, Dr Maria Febbraio (Medical College of Cornell University, Ithaca, NY) for providing the *CD36*-deficient mice, and Dr David Greaves, Dr Richard Siow, and Prof Jeremy Pearson for their helpful discussion of this work.

## References

1. Ross R. Atherosclerosis: an inflammatory disease. *N Engl J Med.* 1999; 340:115–126.
2. Steinberg D. Low density lipoprotein oxidation and its pathobiological significance. *J Biol Chem.* 1997;272:20963–20966.
3. Greaves DR, Gough PJ, Gordon S. Recent progress in defining the role of scavenger receptors in lipid transport, atherosclerosis and host defence. *Curr Opin Lipidol.* 1998;9:425–432.
4. de Villiers DR, Gough PJ, Gordon S. Macrophage scavenger receptors and foam cell formation. *J Leukoc Biol.* 1999;66:740–746.
5. Steinbrecher UP. Receptors for oxidized low density lipoprotein. *Biochim Biophys Acta.* 1999;1436:279–298.
6. Esterbauer H, Gebicki J, Puhl H, Jurgens G. The role of lipid peroxidation and antioxidants in oxidative modification of LDL. *Free Radic Biol Med.* 1992;13:341–390.
7. Frostegard J, Wu R, Giscombe R, Holm G, Lefvert AK, Nilsson J. Induction of T-cell activation by oxidized low density lipoprotein. *Arterioscler Thromb.* 1992;12:461–467.
8. Cushing SD, Berliner JA, Valente AJ, Territo MC, Navab M, Parhami F, Gerrity R, Schwartz CJ, Fogelman AM. Minimally modified low density lipoprotein induces monocyte chemotactic protein 1 in human endothelial cells and smooth muscle cells. *Proc Natl Acad Sci USA.* 1990;87: 5134–5138.
9. Yamaguchi M, Sato H, Bannai S. Induction of stress proteins in mouse peritoneal macrophages by oxidized low-density lipoprotein. *Biochem Biophys Res Commun.* 1993;193:1198–1201.
10. Siow RC, Sato H, Leake DS, Pearson JD, Bannai S, Mann GE. Vitamin C protects human arterial smooth muscle cells against atherogenic lipoproteins: effects of antioxidant vitamins C and E on oxidized LDL-induced adaptive increases in cystine transport and glutathione. *Arterioscler Thromb Vasc Biol.* 1998;18:1662–1670.
11. Nagy L, Tontonoz P, Alvarez JGA, Chen H, Evans M. Oxidized LDL regulates macrophage gene expression through ligand activation of PPARγ. *Cell.* 1998;93:229–240.
12. Ricote M, Li AC, Willson TM, Kelly CJ, Glass CK. The peroxisome proliferator-activated receptor-γ is a negative regulator of macrophage activation. *Nature.* 1998;391:79–82.
13. Jiang C, Ting AAT, Seed B. PPAR-γ agonists inhibit production of monocyte inflammatory cytokines. *Nature.* 1998;391:82–86.
14. Moore KJ, Rosen ED, Fitzgerald KL, Randow F, Andersson LP, Altshuler D, Milstone DS, Mortensen RM, Spiegelman BM, Freeman MW. The role of PPAR-γ in macrophage differentiation and cholesterol uptake. *Nat Med.* 2001;7:41–47.
15. Chawla A, Barak Y, Nagy L, Liao D, Tontonoz P, Evans M. PPAR-γ dependent and independent effects on macrophage-gene expression in lipid metabolism and inflammation. *Nat Med.* 2001;7:48–52.
16. Itoh K, Chiba T, Takahashi S, Ishii T, Igarashi K, Katoh Y, Oyake T, Hayashi N, Satoh K, Hatayama I, Yamamoto M, Nabeshima Y. An Nrf2/small Maf heterodimer mediates the induction of phase II detoxifying enzyme genes through antioxidant response elements. *Biochem Biophys Res Commun.* 1997;236:313–322.
17. Ramos-Gomez M, Kwak MK, Dolan PM, Itoh K, Yamamoto M, Talalay P, Kensler TW. Sensitivity to carcinogenesis is increased and chemoprotective efficacy of enzyme inducers is lost in nrf2 transcription factor-deficient mice. *Proc Natl Acad Sci USA.* 2001;98:3410–3415.
18. Kwak MK, Itoh K, Yamamoto M, Sutter TR, Kensler TW. Role of transcription factor Nrf2 in the induction of hepatic phase 2 and antioxidative enzymes in vivo by the cancer chemoprotective agent, 3*H*-1,2-dimethiole-3-thione. *Mol Med.* 2001;7:135–145.
19. Cho HY, Jedlicka AE, Reddy SP, Kensler TW, Yamamoto M, Zhang LY, Kleeberger SR. Role of Nrf2 in protection against hyperoxic lung injury in mice. *Am J Respir Cell Mol Biol.* 2002;26:175–182.
20. Ishii T, Itoh K, Takahashi S, Sato H, Yanagawa T, Katoh Y, Bannai S, Yamamoto M. Transcription factor Nrf2 coordinately regulates a group of oxidative stress-inducible genes in macrophages. *J Biol Chem.* 2000;275: 16023–16029.
21. Itoh K, Wakabayashi N, Katoh Y, Ishii T, Igarashi K, Engel JD, Yamamoto M. Keap1 represses nuclear activation of antioxidant responsive elements by Nrf2 through binding to the amino-terminal Neh2 domain. *Genes Dev.* 1999;13:76–86.
22. Itoh K, Wakabayashi N, Katoh Y, Ishii T, O'Connor T, Yamamoto M. Keap1 regulates both cytoplasmic-nuclear shuttling and degradation of Nrf2 in response to electrophiles. *Genes Cells.* 2003;8:379–391.
23. Siow RCM, Ishii T, Sato H, Taketani S, Leak DS, Sweiry JH, Pearson JD, Bannai S, Mann GE. Induction of the antioxidant stress proteins heme oxygenase-1 and MSP23 by stress agents and oxidized LDL in cultured vascular smooth muscle cells. *FEBS Lett.* 1995;368:239–242.
24. Wang LJ, Lee TS, Lee FY, Pai RC, Chau LY. Expression of heme oxygenase-1 in atherosclerotic lesions. *Am J Pathol.* 1998;152:711–720.
25. Lee TS, Chau LY. Heme oxygenase-1 mediates the anti-inflammatory effect of interleukin-10 in mice. *Nat Med.* 2002;8:240–246.
26. Kang SW, Chae HZ, Seo MS, Kim K, Baines IC, Rhee SG. Mammalian peroxiredoxin isoforms can reduce hydrogen peroxide generated in response to growth factors and tumor necrosis factor-α. *J Biol Chem.* 1994;91:7022–7026.
27. Jin D-Y, Chae HZ, Rhee SG, Jeang K-T. Regulatory role for a novel human thioredoxin peroxidase in NF-κB activation. *J Biol Chem.* 1997; 272:30952–30961.
28. Leonarduzzi G, Arkan MC, Basaga H, Chiarpotto E, Sevanian, Poli G. Lipid oxidation products in cell signaling. *Free Radic Biol Med.* 2000; 1370–1378.
29. Han J, Hajjar DP, Febbraio M, Nicholson AC. Native and modified low density lipoproteins increase the functional expression of the macrophage class B scavenger receptor, CD36. *J Biol Chem.* 1997;272:21654–21659.
30. Yoshida H, Quehenberger O, Kondratenko N, Green S, Steinberg D. Minimally oxidized low-density lipoprotein increases expression of scavenger receptor A, CD36, and macrosialin in resident mouse peritoneal macrophages. *Arterioscler Thromb Vasc Biol.* 1998;18:794–802.
31. Kawane T, Hou JQ, Sato H, Sugita Y, Bannai S, Ishii T. Induction of metalloelastase mRNA in murine peritoneal macrophages by diethylmaleate. *Biochim Biophys Acta.* 1999;1427:155–160.
32. Glass CK. Potential roles of the peroxisome proliferator-activated receptor-γ in macrophage biology and atherosclerosis. *J Endocrinol.* 2001;169:461–464.
33. Klappacher GW, Glass CK. Roles of peroxisome proliferator-activated receptor γ in lipid homeostasis and inflammatory responses of macrophages. *Curr Opinion Lipdol.* 2002;13:305–312.
34. Tontonoz P, Nagy L, Alvarez JGA, Thomazy VA, Evans RM. PPARγ promotes monocyte/macrophage differentiation and uptake of oxidized LDL. *Cell.* 1998;93:241–252.
35. Ricote M, Huang J, Fajas L, Li A, Welch J, Najib J, Witztum JL, Auwerx J, Palinski W, Glass CK. Expression of the peroxisome proliferator-activated receptor γ (PPAR-γ) in human atherosclerosis and regulation in macrophages by colony stimulating factors and oxidized low density lipoprotein. *Proc Natl Acad Sci USA.* 1998;95:7614–7619.
36. Podrez EA, Poliakov E, Shen Z, Zhang R, Deng Y, Sun M, Finton PJ, Shan L, Febbraio M, Hajjar DP, Silverstein RL, Hoff HF, Salomon RG, Hazen SL. A novel family of atherogenic oxidized phospholipids promotes macrophage foam cell formation via the scavenger receptor CD36 and is enriched in atherosclerotic lesions. *J Biol Chem.* 2002;277:38517–38523.
37. Podrez EA, Hoppe G, O'Neil J, Hoff HF. Phospholipids in oxidized LDL not adducted to apoB are recognized by the CD36 scavenger receptor. *Free Radic Biol Med.* 2003;34:356–364.
38. Febbraio M, Podrez EA, Smith JD, Hajjar DP, Hazen SL, Hoff HF, Sharma K, and Silverstein RL. Targeted disruption of the class B scavenger receptor CD36 protects against atherosclerotic lesion development in mice. *J Clin Invest.* 2000;105:1049–1056.
39. Kavanagh IC, Symes CE, Renaudin P, Nova E, Mesa MD, Boukouvalas G, Leake DS, Yaqoob P. Degree of oxidation of low density lipoprotein

affects expression of CD36 and PPARγ, but not cytokine production, by human monocyte-macrophages. *Atherosclerosis*. 2003;2:271–282.
40. Brasen JH, Hakkinen T, Malle E, Beisiegel U, Yla-Herttula S. Patterns of oxidized epitopes, but not NFκB expression, change during atherogenesis in WHHL rabbits. *Atherosclerosis*. 2003;166:13–21.
41. Jurgens G, Chen Q, Esterbauer H, Mair S, Ledinski G, Dinges HP. Immunostaining of human autopsy aortas with antibodies to modified apolipoprotein B apoprotein(a). *Arterioscler Thromb*. 1993;13:1689–1699.
42. Napoli C, D'Armiento FP, Mancini FP, Postiglione A, Witzum JL, Palumbo G, Palinski W. Fatty streak formation occurs in human fetal aortas and is greatly enhanced by maternal hypercholesterolemia. Intimal accumulation of low density lipoprotein and its oxidation products precede monocyte recruitment into early atherosclerotic lesions. *J Clin Invest*. 1997;11:2680–2690.
43. Bea F, Hudson FN, Chait A, Kavanagh TJ, Rosenfeld ME. Induction of glutathione synthesis in macrophages by oxidized low-density lipoproteins is mediated by consensus antioxidant response elements. *Circ Res*. 2003;92:386–393.
44. Ricciarelli R, Zingg JM, Azzi A. Vitamin E reduces the uptake of oxidized LDL by inhibiting CD36 scavenger receptor expression in cultured aortic smooth muscle cells. *Circulation*. 2000;102:82–87.
45. Matsumoto K, Hirano K, Nozaki S, Takamoto, Nishida M, Malagawa-Toyama Y, Janabi MY, Ohya T, Yamashita S, Matsuzawa Y. Expression of macrophage (Mϕ) scavenger receptor, CD36, in cultured human aortic smooth muscle cells in association with expression of peroxisome proliferator activated receptor-γ, which regulates gain of Mϕ-like phenotype in vitro and its implications in atherogenesis. *Arterioscler Thromb Vasc Biol*. 2000;20:1027–1032.
46. Bishop-Bailey D, Hla T, Warner TD. Intimal smooth muscle cells as a target for peroxisome proliferator-activated receptor-γ ligand therapy. *Circ Res*. 2002;91:210–217.
47. Ikeda Y, Sugawara A, Taniyama Y, Urano A, Igarashi K, Arima S, Ito S, Takeuchi K. Suppression of rat thromboxane synthase gene transcription by peroxisome proliferator-activated receptor γ in macrophages via an interaction with Nrf2. *J Biol Chem*. 2000;275:33142–33150.
48. Kunsch C, Medford RM. Oxidative stress as a regulator of gene expression in the vasculature. *Circ Res*. 1999;85:753–765.

# Protection against electrophile and oxidant stress by induction of the phase 2 response: Fate of cysteines of the Keap1 sensor modified by inducers

Nobunao Wakabayashi*†‡, Albena T. Dinkova-Kostova*, W. David Holtzclaw*, Moon-Il Kang‡, Akira Kobayashi‡, Masayuki Yamamoto‡, Thomas W. Kensler*†, and Paul Talalay*§

*The Lewis B. and Dorothy Cullman Cancer Chemoprotection Center, Department of Pharmacology and Molecular Sciences, School of Medicine, and †Department of Environmental Health Sciences, Bloomberg School of Public Health, The Johns Hopkins University, Baltimore, MD 21205; and ‡Center for Tsukuba Advanced Research Alliance and Japan Science and Technology Agency/Exploratory Research for Advanced Technology Environmental Response Project, University of Tsukuba, 1-1-1 Tennoudai, Tsukuba 305-8575, Japan

Contributed by Paul Talalay, December 12, 2003

**Induction of a family of phase 2 genes encoding for proteins that protect against the damage of electrophiles and reactive oxygen intermediates is potentially a major strategy for reducing the risk of cancer and chronic degenerative diseases. Many phase 2 genes are regulated by upstream antioxidant response elements (ARE) that are targets of the leucine zipper transcription factor Nrf2. Under basal conditions, Nrf2 resides mainly in the cytoplasm bound to its cysteine-rich, Kelch domain-containing partner Keap1, which is itself anchored to the actin cytoskeleton and represses Nrf2 activity. Inducers disrupt the Keap1-Nrf2 complex by modifying two (C273 and C288) of the 25 cysteine residues of Keap1. The critical role of C273 and C288 was established by (*i*) their high reactivity when purified recombinant Keap1 was treated with dexamethasone mesylate and the dexamethasone-modified tryptic peptides were analyzed by mass spectrometry, and (*ii*) transfection of *keap1* and *nrf2* gene-deficient mouse embryonic fibroblasts with constructs expressing cysteine to alanine mutants of Keap1, and measurement of the ability of cotransfected Nrf2 to repress an ARE-luciferase reporter. Reaction of Keap1 with inducers results in formation of intermolecular disulfide bridges, probably between C273 of one Keap1 molecule and C288 of a second. Evidence for formation of such dimers was obtained by 2D PAGE of extracts of cells treated with inducers, and by the demonstration that whereas C273A and C288A mutants of Keap1 alone could not repress Nrf2 activation of the ARE-luciferase reporter, an equal mixture of these mutant constructs restored repressor activity.**

This paper describes the molecular mechanisms that control expression of phase 2 genes, which play central roles in protecting aerobic life against the relentless stresses imposed by electrophiles and reactive oxygen intermediates: the principal causes of many chronic diseases, including cancer. Many phase 2 proteins are enzymes that are highly inducible by transcriptional activation, and exert versatile, long-acting, and often catalytic protection against electrophile and oxidative damage. Phase 2 proteins comprise not only the "classical" phase 2 xenobiotic-metabolizing enzymes such as glutathione transferases and UDP-glucuronosyltransferases, which conjugate xenobiotics with endogenous ligands, but include also NAD(P)H:quinone reductase (NQO1) (EC 1.6.99.2), epoxide hydrolase, heme oxygenase 1, ferritin, γ-glutamylcysteine ligase, glutathione reductase, aldehyde dehydrogenase, dihydrodiol dehydrogenase, leukotriene $B_4$ dehydrogenase, and glutathione *S*-conjugate efflux pumps (reviewed in refs. 1 and 2).

Much evidence supports the notion that induction of the phase 2 response is an efficient strategy for reducing the risk of a variety of diseases (for reviews, see refs. 2–4). For example: (*i*) mice in which the phase 2 response has been silenced (*nrf2* gene knockouts) have low and uninducible phase 2 enzymes, are much more susceptible to carcinogens and the toxicity of oxygen and electrophiles and, unlike cognate wild-type mice, cannot be protected by inducers (2, 5–7). (*ii*) Targeted disruption of two phase 2 enzymes in mice (glutathione transferase π and NQO1) increased incidence of skin tumors evoked by polycyclic hydrocarbons (8, 9). (*iii*) Bioassays of phase 2 inducer potency, based on quantifying NQO1 activity in murine hepatoma cells, resulted in the isolation of several potent anticarcinogenic inducers, including sulforaphane from broccoli, and have also guided the synthesis of potent inducers (for review, see ref. 2). (*iv*) Human populations polymorphic for certain phase 2 enzymes are more susceptible to toxicity and carcinogenesis (10–13). (*v*) Administration of the phase 2 inducer oltipraz to individuals at very high risk of developing primary hepatocellular carcinoma, because of heavy dietary intakes of aflatoxin $B_1$, substantially increased excretion of phase 2 metabolites of aflatoxin, a biomarker for carcinogen load (14).

Inducers of phase 2 genes belong to nine structurally highly diversified chemical classes (15, 16), and share only a few common properties (17): (*i*) all are chemically reactive; (*ii*) nearly all are electrophiles; (*iii*) most are substrates for glutathione transferases; and (*iv*) all can modify sulfhydryl groups by alkylation, oxidation, or reduction. Recognition of these properties suggested that cells contain primary sensor(s) equipped with highly reactive cysteine residues that are recognized and chemically modified by inducers, thereby initiating the enhanced transcription of phase 2 genes. We have recently obtained evidence that Kelch-like ECH-associated protein 1 (Keap1) is probably this regulatory sensor (18), a conclusion that is strongly supported by the accompanying paper (19), and other very recent studies (20, 21).

Phase 2 genes are regulated by 5′ upstream regulatory sequences which have been designated as antioxidant response elements (ARE) (22, 23). Nrf2, a member of the NF-E2 family of nuclear basic leucine zipper transcription factors, binds to the ARE, and accelerates transcription of the cognate genes (24–26). Under basal conditions, Keap1, a recently identified protein associated with the actin cytoskeleton, binds very tightly to Nrf2, anchors this transcription factor in the cytoplasm, and targets it for ubiquitination and proteasome degradation, thereby repressing the ability of Nrf2 to induce phase 2 genes (27–32). Inducers disrupt the Keap1-Nrf2 complex, allowing Nrf2 to translocate to the nucleus where, in heterodimeric combinations with other

Abbreviations: ARE, antioxidant response element; NQO1, nicotinamide quinone oxidoreductase 1, NAD(P)H:quinone acceptor oxidoreductase 1; KONO, *nrf2/keap1* double knockout; Dex-mes, dexamethasone 21-mesylate; Keap1, Kelch-like ECH-associated protein 1; IVR, intervening region of Keap1: C257A, C257 replaced by alanine; C257A–C297A, all cysteine residues from C257 to C297 replaced by alanine.

§To whom correspondence should be addressed at: Department of Pharmacology and Molecular Sciences, The Johns Hopkins University School of Medicine, 725 North Wolfe Street, Baltimore, MD 21205. E-mail: ptalalay@jhmi.edu.





www.pnas.org/cgi/doi/10.1073/pnas.0307301101

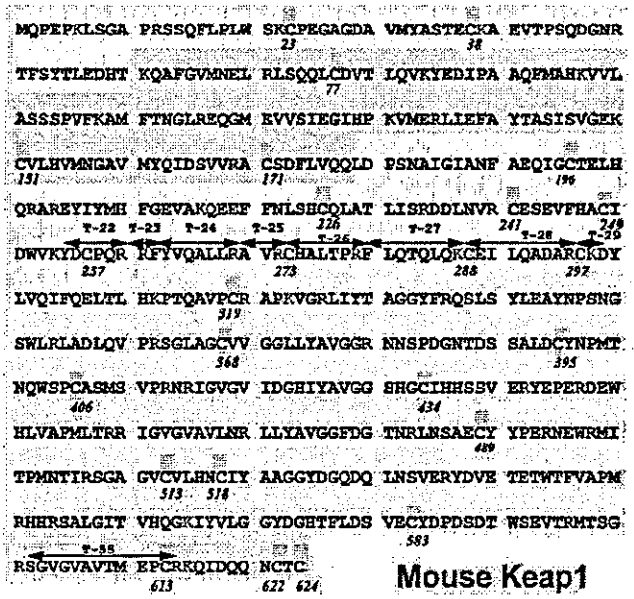


Fig. 1. Amino acid sequence of the five domains of Keap1: (*i*) N-terminal region (NTR, amino acids 1–60: two cysteines, blue). (*ii*) BTB (Broad complex, Tramtrack, Bric-a-Brac; amino acids 61–179: three cysteines, pink), an evolutionarily conserved protein–protein interaction motif that often dimerizes with other BTB domains (33). (*iii*) IVR (amino acids 180–314: eight cysteines, yellow). (*iv*) Double glycine (DGR, amino acids 315–598: nine cysteines, gray) comprising six Kelch motifs (amino acids 315–359, 361–410, 412–457, 459–504, 506–551, and 553–598). Repeated Kelch motifs give rise to a $\beta$-propeller structure with multiple protein-binding sites (34). The DGR of Keap1 binds tightly to the Neh2 segment (the 100 N-terminal amino acids) of Nrf2 (24, 27), and is also the region involved in anchoring Keap1 to the actin cytoskeleton (19). (*v*) C-terminal region (CTR, amino acids 599–624: three cysteines, green). The 25 cysteine residues are highlighted in bright yellow, the 39 arginine residues are blue, and the 17 lysine residues are red. The tryptic peptides labeled with dexamethasone (T-22, T-26, T-28, T-29, and T-55) are designated. The matrix-assisted laser desorption ionization/time-of-flight mass spectral analyses of all 57 tryptic peptides, including the 19 peptides that contain cysteine residues are recorded in Table 1 (see *Supporting Text*).

basic leucine zipper proteins, it binds to AREs of phase 2 genes and accelerates their transcription.

The 624 amino acids of murine Keap1 include 25 cysteines and comprise five domains (Fig. 1). Because all cysteine residues are conserved, identification of those critical for induction presented special problems. Consequently, we resorted to the strategy of first identifying the most reactive cysteines by chemical modification with dexamethasone 21-mesylate (Dex-mes), an inducer that reacts irreversibly with thiols, and second, examining whether mutations of these residues alter the ability of Keap1 to repress Nrf2 function. Four cysteines [C257, C273, C288, and C297, all located in the intervening region (IVR) domain] of purified recombinant Keap1 were most reactive with Dex-mes (18), suggesting strongly that Keap1 is the molecular sensor for inducers. We now establish the critical functional role of these reactive cysteine thiols of Keap1 in signaling induction, by further analysis of the Dex-mes-modified tryptic peptides of Keap1, and by introducing systematic mutations of these cysteine residues.

## Experimental Procedures

**Constructs.** Each Cys to Ala mutant of Keap1 was produced by PCR and standard recombination techniques. Construct authenticity was confirmed by sequencing. pcDNA3 or pET vectors were used for mammalian or bacterial cell expression, respectively, as described (18). All primers and PCR conditions used for genotyping and for the preparation of the constructs used in this study are listed in *Supporting Text*, which is published as supporting information on the PNAS web site.

**Production of *keap1*(−/−) and Combined *keap1*(−/−)::*nrf2*(−/−) Mouse Embryonic Fibroblasts.** Fibroblasts were isolated from 13.5-day-old embryos of *keap1*(−/−) and *keap1*(−/−)::*nrf2*(−/−) mice and used to establish stable lines by standard procedures (35). Cells were maintained in Iscove's modified Eagle's medium, supplemented with 10% heat-inactivated FBS, at 37°C and 5% $CO_2$.

**Functional Reporter Assay.** Transient reporter assays were performed by standard transfection methods using $2 \times 10^5$ *keap*(−/−)::*nrf2*(−/−) mouse embryonic fibroblast (MEF) cells (K0N0) in 60-mm diameter dishes. Each construct of plasmid [2 $\mu$g of reporter gene pNQO1AREluc, 2 $\mu$g of pRLTK-normalizing vector, 8 $\mu$g of pCMVmNrf2, and various amounts (see Fig. 4) of each Keap1 expression vector, with total DNA adjusted to 2 $\mu$g with pcDNA3] was introduced into K0N0 MEF cells by the calcium phosphate co-precipitation method. Two micrograms of pRLTK plasmid bearing the *Renilla* luciferase gene under the control of the HSV-tk promoter/enhancer were included in each transfection and used for normalization. Cells were harvested 24 h after transfection and luciferase activities were measured according to the manufacturer's instructions (Promega). Relative luciferase activity was obtained from six independent transfection experiments and is shown ±SEM in each figure.

**Nonreducing-Reducing 2D SDS/PAGE.** HEK293 cells ($5 \times 10^5$ per 60-mm dish) were transfected with 20 $\mu$g of pEFmKeap1. After transfection (48 h), the medium was exchanged with serum-free medium containing 250 $\mu$M DTT, and cells were incubated for 3 h. After extensive washing with PBS (5×), cells were exposed to an inducer or vehicle and incubated in medium at 37°C, 5% $CO_2$ for 6 h, and finally harvested with 150 $\mu$l of RIPA buffer (10 mM Tris·HCl, pH 7.5/1% Nonidet P-40/0.1% Na-deoxycholate/0.1% SDS/150 mM NaCl/1 mM EDTA). Samples were boiled with DTT-free SDS buffer, and 25 $\mu$g of protein were subjected to nonreducing disk-gel (2-mm diameter disk) SDS/PAGE. Gels were ejected and reduced with 1× SDS buffer including 5% 2-mercaptoethanol at room temperature for 1 h, with one buffer change. Disk gels were inserted into the well of a second SDS/PAGE and subjected to electrophoresis.

**Immunoblotting.** Keap1 was detected by using rabbit anti-mKeap1 polyclonal antibody (25, 28). For normalizing cell number, nuclear Lamin B was detected from the same extracts with goat anti-Lamin B antibody (Santa Cruz Biotechnology). For normalizing transfection efficiency, Bsd-GFP protein, encoded from the same plasmid as Keap1, was detected by goat anti-GFP antibody (Santa Cruz Biotechnology). Membranes were blocked and treated with primary antibody followed by reaction with the appropriate secondary antibodies conjugated to horseradish peroxidase (Zymed, Bio-Rad). Immune complexes were visualized with enhanced chemiluminescence (Amersham Pharmacia).

## Results and Discussion

**Identification of the Most Reactive Cysteine Residues of Keap1 and Their Importance for Inducer and Nrf2-Binding Activity.** In further validation that Keap1 contains highly reactive cysteine thiols that sense inducers (18), we carried out additional experiments with Dex-mes, an inducer which alkylates thiols irreversibly, and increases their masses substantially (374.19 atomic mass units). Homogeneous recombinant Keap1 (600 pmol) was incubated with a modest excess of Dex-mes (6 nmol) at 25°C and pH 8.0,

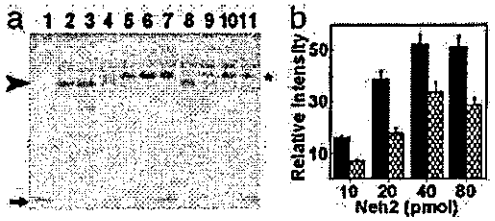


Fig. 2. Comparison of binding of wild-type and mutant (C257A–C297A) Keap1 to the Neh2 domain of Nrf2. (*a*) Native gel electrophoresis showing complex between Keap1 (100 pmol) and the Neh2 domain of Nrf2 (10, 20, 40, and 80 pmol, lanes 4–7 and 8–11, respectively). Lane 1, Neh2; lane 2, wild-type Keap1; lane 3, mutant Keap1. Lanes 4–7 show progressively increasing quantities of complex between wild-type Keap1 and Neh2; lanes 8–11 show lower quantities of complex formation between mutant Keap1 and Neh2. Arrowhead, arrow, and asterisk show Keap1, Neh2, and Neh2-Keap1 or mutant Keap1 complex bands, respectively. (*b*) Densitometric quantification of the intensities of bands of complexes between Neh2 and wild-type Keap1 (black bars) and mutant Keap1 (hatched bars).

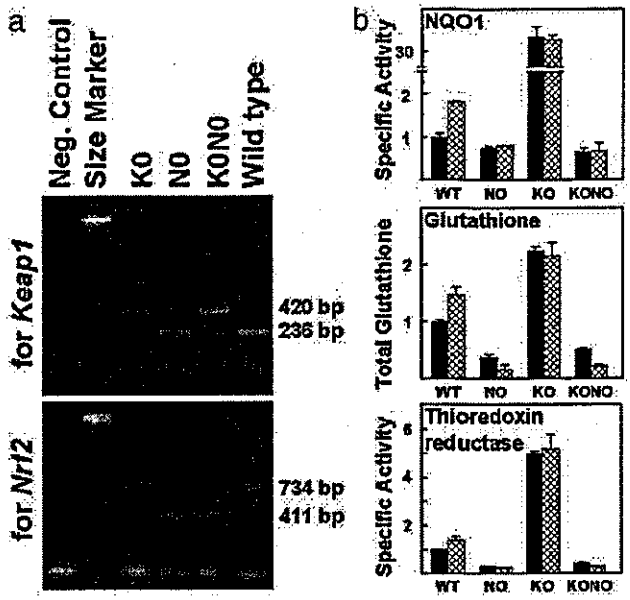


Fig. 3. Genotyping and levels of expression of phase 2 gene products in established lines of embryonic fibroblasts obtained from mice in which the *keap1* (K0), *nrf 2* (N0), or both genes (K0N0) were disrupted. (*a*) Electrophoresis of the PCR products derived from *keap1* wild-type (236 bp) and mutant (420 bp) alleles, and *nrf2* wild-type (734 bp) and mutant (411 bp) alleles. (*b*) Comparison (normalized to wild-type controls) of the specific activities of NQO1 and thioredoxin reductase, and concentration of glutathione in cell-free extracts of the three mutant and wild-type mouse embryonic fibroblasts. Black bars, cells untreated with inducers; hatched bars, cells exposed for 24 h to 1.5 μM sulforaphane.

for 2 h. Excess Dex-mes was removed by gel filtration, and the denatured protein was treated with *N*-ethylmaleimide to alkylate unreacted thiols. Tryptic peptides were separated by reversed-phase HPLC, fractions were analyzed by matrix-assisted laser desorption ionization/time-of-flight (MALDI-TOF) MS. The 57 tryptic peptides were designated T-1 to T-57. All of the predicted 19 cysteine-containing tryptic peptides were recovered in the fractions (either as single peptides or as incompletely cleaved di- or tripeptides). Their masses agreed within 0.5 atomic mass units with calculated values (see Table 1, which is published as supporting information on the PNAS web site). Peptides containing C257 (T-22), C273 (T-25 to T-28), C288 (T-28), C297 (T-29), and C613 (T-55) (see Fig. 1) were found to have mass increases corresponding to the covalent addition of the steroid. All other cysteine-containing peptides showed mass increases of 125.05 atomic mass units (for each cysteine residue), indicating alkylation by *N*-ethylmaleimide. Thus, in agreement with our earlier findings, C257, C273, C288, and C297, all located in the IVR domain, as well as C613, are the most reactive cysteine residues of native Keap1 *in vitro* (18).

The reproducible labeling of 4 specific cysteines of Keap1 prompted us to examine the properties of recombinant Keap1 in which these cysteine residues were replaced by alanine. The mutant protein (C257A–C297A) was overexpressed in *E. coli* and purified to homogeneity by our procedure used to purify wild-type Keap1 (18). Both wild-type and mutant proteins migrated identically on native and SDS/PAGE (molecular weight ≈ 65,000).

Comparison of rates of binding of [$^3$H]Dex-mes and sulforaphane to purified wild-type and mutant (C257A–C297A) Keap1, measured by tritium incorporation and dithiocarbamate formation, respectively, revealed that the reaction rates of the mutant were ≈50% slower, confirming that the modified cysteines were indeed the most reactive in the native protein.

We next examined whether the four most reactive cysteine residues of Keap1 influenced binding to Nrf2. Incubation of Keap1 with the Neh2 (Keap1 binding) domain of Nrf2 under reducing conditions led to formation of a complex that can be detected by native PAGE (Fig. 2*a*). At a constant Keap1 concentration, the intensity of the band corresponding to the complex increases with increasing amounts of Neh2, reaching saturation at a ratio of Keap1 to Neh2 of ≈2:1. Both wild-type and mutant Keap1 can form complexes with Neh2, but the mutant protein has ≈50% lower affinity for Neh2 based on band density (Fig. 2*b*).

Two separate lines of evidence, rates of reaction with inducers and binding to the Neh2 domain, indicate that the mutant Keap1 in which four specific cysteine residues in the IVR (C257A–C297A) were mutated not only reacted markedly more slowly with inducers, but also displayed a parallel decrease in affinity for the Neh2 domain of Nrf2. This is powerful evidence for the importance of these cysteines of Keap1 for repression of Nrf2.

**Preparation and Properties of Mouse Embryonic Fibroblasts in Which *keap1*, *nrf2*, or both Genes Have Been Disrupted.** Further understanding of the regulatory functions of Keap1 and its mutants by transfection analyses of whole cells required cell lines in which interference from endogenous Keap1 and Nrf2 was eliminated. Consequently, we established cell lines from primary cultures of embryo fibroblasts of wild-type, *nrf2*-knockout (N0), *keap1*-knockout (K0), and K0N0 mice (36) (Fig. 3*a*). Wild-type cells have readily detectable basal levels of NQO1, glutathione, and thioredoxin reductase, which were elevated upon exposure to 1.5 μM sulforaphane (Fig. 3*b*). N0 and K0N0 cells have lower and essentially uninducible levels of these components. Moreover, the already lower levels of glutathione were further reduced by >50% upon treatment with sulforaphane, most likely because of direct conjugation with reduced glutathione (37). In sharp contrast, K0 cells have much higher basal levels compared to their wild-type counterparts, and essentially no induction was observed upon exposure to sulforaphane. These findings confirm the critical role of the Keap1/Nrf2 system for both basal and inducible expression of these phase 2 responses, and are consistent with the proposed repression of Nrf2 by Keap1.

**Repression by Keap1 of ARE- and Nrf2-Dependent Gene Expression: Mutations of Cysteine Residues of Keap1.** Effects of specific cysteine to alanine mutations on the ability of Keap1 to repress Nrf2 *in*

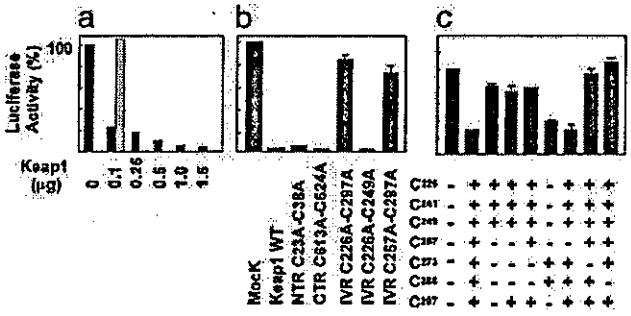


Fig. 4. Repression of the intensity of luciferase luminescence of ARE-luciferase in K0N0 mouse embryonic fibroblasts by wild-type Keap1 and its cysteine mutants. All cells were transfected with the ARE-luciferase (2 μg) and the Nrf2 (8 μg) constructs. (*a*) Repression of luminescence as a function of amount of wild-type Keap1 (black bars) and its reversal by exposure to 2 μM sulforaphane (gray bar). (*b*) Repression of luminescence by wild-type (WT) Keap1 (2 μg) and equivalent quantities of the following mutants: NTR (C23A and C38A); CTR (C613A, C622A, and C624A); IVR C226A–C297A (C226A, C241A, C249A, C257A, C273A, C288A, and C297A); IVR C226A–C249A (C226A, C241A, and C249A); and IVR C257A–C297A (C257A, C273A, C288A, and C297A). (*c*) Repressive activity of single or multiple cysteine mutants of Keap1 with 100 ng of each expression vector. The structures of the mutants are designated: + for cysteine, − for alanine. The structure of each wild-type and mutant Keap1 is shown below the bar indicating its repressor activity. Repressor activity is abrogated if C273 or C288, or both, are mutated to alanine.

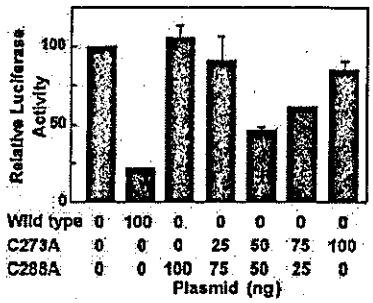


Fig. 5. Repression of the intensity of luciferase luminescence of ARE-luciferase in K0N0 mouse embryo fibroblasts by wild-type Keap1 and its C273A and C288A mutants. All cells were transfected with the ARE-luciferase (2 μg) and the Nrf2 (8 μg) constructs. The luminescence observed in the absence of Keap1 is expressed as 100 units. Addition of 100 ng of wild-type Keap1 plasmid reduced the luminescence to ≈20%. The plasmids (100 ng) coding for C273A or C288A showed little, if any, repression of the fluorescence, whereas mixtures of these plasmids restored the repressor activity. A mixture of 50 ng of each plasmid repressed ≈40% of the luminescence of the system.

*vivo* were examined by transient transfection experiments in mouse embryonic fibroblasts from *keap1/nrf2* double knockout animals (K0N0). K0N0 cells were transiently transfected with controlled quantities of three vectors: (*i*) an Nrf2 expression vector (pCMVmNrf2); (*ii*) a vector that expresses either wild-type or mutants of Keap1; and (*iii*) a luciferase reporter vector controlled by the ARE of NQO1 (pNQO1AREluc) (38). The effect of mutating cysteine residues of Keap1 on the luciferase activity provided a measure of how such mutations affect repressor function.

Because Keap1 contains 25 cysteine residues, mutation of all possible combinations of cysteine residues was impractical, and we therefore mutated cysteines in selected domains. The BTB and DGR domains of Keap1 (see Fig. 1) are involved in dimerization (33) and Nrf-2/actin binding (19, 27), respectively; consequently, we did not mutate cysteine residues in these regions. The following groups of cysteine to alanine mutations were generated in Keap1: (*i*) N-terminal region (NTR), i.e., C23A and C38A, (*ii*) C-terminal region (CTR), i.e., C613A, C622A, and C624A, (*iii*) seven cysteines in the IVR, and (*iv*) 10 other combinations of mutations of these residues. Control cells were "mock" transfected with all constructs including the Keap1 expression vector, which lacked the cDNA sequence for Keap1.

In the absence of Keap1, the luciferase reporter of transfected cells showed high levels of luminescence (Fig. 4*a*). In agreement with previous studies (27), expression of increasing amounts of wild-type Keap1 in the presence of a constant amount of Nrf2 repressed the ARE-driven reporter luciferase activity in a concentration-dependent manner, and this repression was reversed by sulforaphane (Fig. 4*a*). Mutations of all cysteines in the N-terminal (NTR) or C-terminal (CTR) domains had no effect on the repressor activity of Keap1 (Fig. 4*b*). Thus, although C613 was labeled by Dex-mes, it is apparently not critical for the binding of Keap1 to Nrf2. In sharp contrast, mutants of Keap1 lacking either seven cysteine residues of the IVR (C226A–C297A), or four of these cysteines (C257A–C297A) cannot repress the expression of the luciferase reporter (Fig. 4*b*). This finding strongly suggests that the cysteine residues of Keap1 that are most reactive with an inducer are also those that influence binding and repression of Nrf2.

We next refined the mutation strategy to focus on the effects of mutating various combinations of the aforementioned seven cysteine residues of the IVR. Again mutation of both C226A–C257A and C297A did not disturb repressor activity, nor did mutation of C257A alone. The critical finding (Fig. 4*c*) is that absence of either C273 or C288 (or both) abrogates the repressor activity. Both of these cysteines react avidly with Dex-mes. C273 and C288 are flanked by basic amino acids (RC273H, and KC288E, respectively; see Fig. 1) which lower their $pK_a$ values markedly, and thereby increase their reactivity (39). These results are pleasingly consistent with two very recent studies: Zhang and Hannink (21) showed that C273 or C288 are required for Keap1-dependent ubiquitination of Nrf2, and Levonen *et al.* (20) demonstrated that reactive thiols of Keap1 are targets of electrophilic lipid oxidation products, and mutation of C273 or C288 to serine renders Keap1 unable to prevent Nrf2 nuclear translocation.

The question of how mutation of either C273 or C288 could lead to loss of repressor function was further illuminated by experiments in which mixtures of vectors expressing each of these mutants were transfected simultaneously into the reporter system (Fig. 5). The striking finding was that, whereas each Keap1 mutant alone lacked repressor activity, transfection of a mixture of equal quantities of both of these Keap1 mutant expression vectors led to substantial restoration of repressor activity. This observation supports the view that Keap1 acts as a dimer and suggests that the simultaneous presence of C273 on one monomer and C288 on the other is compatible with repressor activity.

**Formation of Intermolecular Disulfide Bonds by Binding of Phase 2 Enzyme Inducers to Keap1 in Cells.** Our previous observation that reaction of Keap1 with stoichiometric equivalents of dipyridyl disulfide led to formation of two equivalents of pyridine thione (18) strongly suggested that the initially formed mixed disulfide between reagent and protein was rapidly reduced by another highly reactive cysteine thiol of Keap1 to form a disulfide linkage. To determine the oligomerization state of Keap1 after inducer treatment, we first transfected human embryonic kidney (HEK) 293 cells with the Keap1 vector and then exposed the cells to inducers for 6 h in serum-free medium. Inducers of three different types were used, i.e., the Michael reaction acceptor bis(2-hydroxybenzylidene)acetone, the isothiocyanate sulfora-